U.S. DEPARTMENT OF ENERGY

PNNL-18539

Prepared for the U.S. Department of Energy
under Contract DE-AC05-76RL01830

Calibration of a Neutron Hydroprobe for Moisture Measurements in Small-Diameter Steel-Cased Boreholes

AL Ward
RS Wittman

August 2009

Pacific Northwest
NATIONAL LABORATORY

Proudly Operated by Battelle *Since 1965*

DISCLAIMER

PACIFIC NORTHWEST NATIONAL LABORATORY
operated by
BATTELLE
for the
UNITED STATES DEPARTMENT OF ENERGY
under Contract DE-AC05-76RL01830

PNNL-18539

Calibration of a Neutron Hydroprobe for Moisture Measurements in Small-Diameter Steel-Cased Boreholes

AL Ward[1]
R Wittman[2]

[1]Hydrology Group
[2]Radiochemical Sciences and Engineering Group

August 2009

Prepared for
the U.S. Department of Energy
under Contract DE-AC05-76RL01830

Pacific Northwest National Laboratory
Richland, Washington 99352

Acknowledgments

I wish to thank Jim Fields of Washington River Protection Solutions and Curt Wittreich of CH2M Hill Plateau Remediation Company, LLC for supporting this work as well as the staff at S.M. Stoller Corporation, who provided schematics of probe geometry and field calibration data and were always available to answer questions related to data collection and logging operations. Thanks to Rick McCain in particular for providing schematics on the hydroprobe construction and engaging in helpful discussions that helped to focus the model simulations.

Executive Summary

Computation of soil moisture content from thermalized neutron counts requires a calibration relationship, but none exists for 2-in. tubes installed at the Tank T-106 interim barrier. A number of calibration options are available for the neutron probe, including vendor and field calibration, but none of these methods were deemed appropriate for the configuration of interest. The objective of this work was to develop a calibration relation for converting neutron counts measured in 2-in. access tubes to volumetric soil water content, θ. The calibration method chosen for this study was a computational approach based on Monte Carlo techniques. The Monte Carlo N-Particle Transport Code (MCNP), developed by Los Alamos, was chosen to perform the theoretical analyses of neutron diffusion in air, the probe shield, and in the Hanford calibration models. Model calibration was performed using field measurements in the calibration models with 6-in. access tubes.

The mean 16-s neutron count measured in air was 43, the mean count for Model F ($\theta = 0.05$ m^3m^{-3}) was 1515, and Model E ($\theta = 0.117$ m^3m^{-3}) and Model G ($\theta = 0.198$ m^3m^{-3}) generated mean 16-s counts of 2264 and 2887, respectively. The shield count, N_s, typically used as a standard count to compute the count ratio (CR), was 6168. The best-fit model relating water content to neutron counts was an exponential model that was essentially equivalent to that currently being used for 6-in. steel-cased wells. The MCNP simulations successfully predicted N_s for the neutron shield and counts N in the three calibration models for which data were collected in the field. However, predicted counts for air, N_a, (mean 16-s count= 14) were about 65% lower than the measured counts (mean 16-s count =43). This discrepancy can be attributed to uncertainties in the configuration used for the air measurements. MCNP-simulated counts for the physical models were essentially equal to the measured counts with values of 2370, 1515, and 2840 for models E, F, and G, respectively. Successful prediction of the response in 6-in. casings in the three calibration models was motivation to predict the response in 2-in. access tubes.

Simulations were performed for six of the seven calibration models as well as four virtual models with the entire set covering a moisture range of 0 to 0.40 m^3m^{-3}. Predicted counts for the calibration models with 2-in. access tubes were 40 to 50% higher than in the 6-in. tubes. Differences between the 2-in. and 6-in. tube are attributed to the differences in the measurement geometry. The best-fit model relating θ to CR is of the form $\theta = e^A \cdot CR^B$ with A=-1.6622 ± 0.0173 and B=1.8648 ± 0.0522 and r^2= 0.9998. It is recommended that the calibration function based on the CR, rather than N, be used to avoid the local environmental effects that may arise because of the conditions at the time of measurement. Shield counts are sensitive to the conditions of the surrounding environment and are not the most ideal as a standard. A better standard may be a water drum. Application of an existing calibration developed for 6-in. wells resulted to N measurements at the interim barrier predicted water contents ranging from 0.004 to 1.03 m^3 m^{-3} with a mode of 0.166 m^3 m^{-3}. Water contents predicted with the new MCNP-based calibration for the 2-in. wells 2-in. ranged from 0.002 to 0.201 m^3 m^{-3} with a mode of 0.04 m^3 m^{-3}. This is more consistent with the observed range of 0.04 and 0.40 m^3 m^{-3} and a mode of 0.05 m^3 m^{-3} observed in Hanford Formation Sediments. These results suggest that the MCNP code can be used to extend calibrations for the neutron probe to different conditions, including access tube size as well as composition, without the need to construct additional physical models.

Acronyms and Abbreviations

ASTM	American Society for Testing and Materials
cpm	counts per minute
CPN	Campbell Pacific Nuclear
cps	counts per second
CR	count ratio
ENDF/B-VI	Evaluated Nuclear Data File
eV	electron volts
IAEA	International Atomic Energy Agency
KeV	thousand electron volts
MCNP	Monte Carlo N-Particle Transport Code
MeV	million electron volts
N_a	Neutron counts in air
N_s	Neutron counts in probe shield
N	Neutron counts in soil or calibration standard
PNNL	Pacific Northwest National Laboratory

Contents

Figures

Tables

1.0 Introduction

Engineered barriers are designed to control the infiltration of meteoric water through the surface to underlying waste. Such a reduction in infiltration eliminates the major driving force for the transport of mobile contaminants through the vadose zone to the water table. In the typical design, infiltration is reduced by a surface soil layer that stores water for subsequent release to the atmosphere by evapotranspiration (Ward et al. 1997, 2005, 2008). While the need to minimize infiltration through Hanford tank farm surfaces is recognized, typical barrier designs may not be applicable.

An innovative approach to minimizing recharge in tank farms was recently demonstrated in the form of an interim barrier at Hanford's T Tank Farm. The interim barrier consists of a 70,000-ft^2 impermeable polyurea layer that was placed over Tank T-106 and portions of eight adjacent tanks. Polyurea is an impermeable material, similar to that used for truck-bed liners. The temporary barrier was installed under terms of the Tri-Party Agreement and is one of several interim measures to mitigate the migration of vadose zone contaminants resulting from previous tank leaks. The barrier is composed of multiple layers, including a layer of clean Hanford soil overlain by a geotextile layer and a 0.25-in.-thick layer of polyurea at the surface. The soil is up to 3 ft thick on the south end of the covered region and slopes gradually to the north. Numerical modeling suggests that an impermeable layer will eliminate the infiltration of meteoric water and consequently reduce the rate of downward movement of antecedent water and transport of contaminants (McMahon 2007). The interim barrier is intended to remain in place until a final closure decision is reached for the entire tank farm. During installation of the interim barrier, a number of instruments were emplaced beneath the barrier to monitor performance and determine its effectiveness (Zhang et al. 2007). Four instrument nests, each including a multi-segment capacitance probe for automated water soil content measurements, heat-dissipation units for automated matric potential measurements, and a 2-in. carbon steel access tube for manual water content measurements by neutron hydroprobe were installed. Volumetric soil moisture content, θ, in the vadose zone beneath the barrier is one of the primary variables being monitored to assess effectiveness. Accurate measurements of soil water content are therefore needed to determine barrier efficiency. Computing soil moisture content from neutron probe counts requires a calibration relationship.

1.1 Calibration Methods

Probe calibration provides a quantitative link between the neutron counts in soil or a calibration standard, N, (typically in counts per unit time; e.g., counts per second [cps]) and soil volumetric water content, θ. The most accurate calibration functions are those that consider the thermal neutron capture cross section of the access tube, access tube diameter, and tube wall thickness. Accurate calibration also requires considering probe geometry and configuration, including the type of neutron detector and the chemical composition and bulk density of soil. As such, each soil will have a specific calibration function for a particular neutron probe. A number of calibration options are available, including vendor calibration, field calibration, and theoretical calibrations based on neutron diffusion theory.

1.1.1 Vendor Calibration

Vendor calibration curves are developed at the factory. These curves are typically derived from measurements in sealed drums filled with sand equilibrated to different water contents. The access tube is

typically constructed of 2-in.-diameter aluminum tube. Probes developed for the agriculture industry are characterized by a short source-to-detector spacing, and the vendor calibration function relating θ to CR is typically linear (Schwanki et al. 1995). Probes developed for the petroleum industry are characterized by long source-to-detector spacing, and the calibration function relating θ to CR is typically non-linear (Alger et al. 1971; Wilson and Wichmann 1974). The neutron probe used for logging the interim barrier is identical to that used in the agricultural industry. The vendor calibration function is useful for measuring changes in θ, i.e., Δθ, but is less applicable to determining absolute values of θ. Because calibration functions are typically developed for aluminum access tubes, vendor calibration curves are not appropriate for use with access tubes constructed of different diameters or materials. It has been shown that factory calibrations are often inaccurate (e.g., Bell and McCulloch 1969; Rawls and Asmussen 1973; Vachaud et al. 1977; Carneiro and Jong 1985; Chanasyk and Naeth 1996). Silvestri et al. (1991) reported that the calibration curve supplied by the manufacturer was only applicable for sandy soils in which volumetric water contents ranged between 0 and 33%. Calibration is therefore necessary for each type of soil, access tube, and different measuring locations with respect to the soil surface and water table.

1.1.2 Field Calibration

Field calibration is accomplished by the sequential insertion of access tubes directly into the soil or sediment and recording N as the tube advances. Water contents are independently determined from sediment samples collected at the same depths as N is measured during tube advancement or from samples collected adjacent to the access tube. This procedure is repeated using several access tubes per sampling event to obtain a statistically significant number of replicated sets of observations of θ and N within a soil profile for a given distribution θ. Developing a calibration relationship representative of the range of moisture conditions for the site therefore requires installing multiple tubes and collecting samples over the entire range of potential soil water contents to be monitored under field investigations. It is unlikely to find a wide range of water contents under natural conditions, especially in arid environments like those at Hanford (Ward et al. 2000). In arid regions, the range of water content may also be limited at the drier end. Except in the near surface where the soil can dry excessively because of evaporation, the soil water content does not typically decrease much below the permanent wilting point. In layered soils, the rate of drying is dependent on texture, resulting in a non-uniform distribution of θ that can increase the error in the calibration function. This limitation can be overcome by irrigating the soil to change the moisture content.

1.1.3 Rapid Field Calibration

Carneiro and De Jong (1985) described a quick field calibration method based on measuring CR during the application of known amounts of irrigation water. The slope *b* of the calibration function is determined from the equation:

$$b = \frac{S_f - S_i}{\sum_{i=1}^{n} N_f \cdot \Delta z - \sum_{i=1}^{n} N_i \cdot \Delta z} \tag{1.1}$$

where S_f is the final soil water storage calculated from the soil surface down to the depth of the wetting front, z; S_i is the initial soil water storage to depth z; and N_f and N_i are the final N corresponding to depth

increases, Δz, respectively. Because the change in soil water storage corresponds to the applied irrigation water depth, the difference (S_f - S_i) is known, and *b* of the calibration curve is known. The value of *a* is calculated from:

$$a = \theta - b \cdot N \tag{1.2}$$

in which the value of θ was obtained from soil samples taken from the field at the time N was measured. Water content is determined by gravimetric methods in the laboratory. A calibration approach requiring the application of supplemental water is unlikely to be acceptable in tank farms and other waste management sites.

1.1.4 Theoretical Models

Calibration relationships have also been developed based on the theoretical analysis of neutron diffusion in different material, including soils and rock (e.g., Cotecchia et al. 1968; Couchat et al. 1975; Vachaud et al. 1977; Goncalves et al. 1994). Couchat et al. (1975) described a neutron capture model for calibration based on the simulation of neutron absorption and diffusion in a graphite pile. This approach yielded a linear calibration function that depended on soil moisture and bulk density. One advantage of this method is that it allows corrections to be made when the soil bulk density changes. However, this is only true if the change is due to a change in pore volume, not if bulk density changes are due to differences in the composition of the soil phase. This calibration method does not account for the escape of neutrons from the soil surface when z < 15 cm. Analytical solutions of radiation transport problems, however, are not applicable to the complicated geometries found in most cases of practical interest.

The calibration of neutron moisture gauges can also be accomplished using Monte Carlo simulation techniques. The Monte Carlo N-Particle Transport Code (MCNP), developed by Los Alamos, is one of the more widely used tools used for comprehensive, theoretical analyses of neutron diffusion. MCNP has been used to simulate nuclear processes, including particle interactions involving neutrons, photons, electrons, and coupled neutron/photon/electron transport. Although the most common applications are related to reactor design, radiation protection, and medical physics, it has also been used extensively in nuclear oil well logging. The code treats an arbitrary three-dimensional configuration of materials in geometric cells bounded by first- and second-degree surfaces and fourth-degree elliptical tori. Point-wise cross-section data are often used, although group-wise data also are available. MCNP includes an extensive collection of cross-section data, a flexible tally structure, and a variety of variance reduction tools. The tally cards are used to specify the type of information generated by the simulation, including current across a surface, flux at a point, or energy deposition averaged over a cell. Simulating neutron diffusion accounts for all reactions given in a particular cross-section evaluation. MCNP uses the Evaluated Nuclear Data File (ENDF/B-VI), a core nuclear reaction database containing evaluated cross sections, spectra, angular distributions, fission product yields, thermal neutron scattering, and photo-atomic and other data, with emphasis on neutron-induced reactions.

1.1.5 Effects of Borehole Configuration

There are over 8000 wells at the Hanford Site, including vadose zone and groundwater wells. These wells were completed with a variety of casing configurations with variations in casing diameter, casing thickness, and multiple construction or completion casings such as telescoping casings. Neutron

attenuation due to casing thickness cannot be easily quantified because of the distribution of the neutron cloud and its subsequent migration (Meisner, 1995; Engleman et al. 1995; Meisner et al. 1996). Owing to a factor of four difference in the scattering cross-section of thermal neutrons and iron (in steel casing), a neutron travelling from the formation towards the detector can undergo an elastic collision and be directed away from the detector. A neutron can therefore cause an increase as well as a decrease in the observed CR observed for increasing casing thickness. Borehole configuration can have a significant effect on the response of the hydroprobe to variations in water content outside the borehole. The material used as a sealant between multiple casings and in the annulus between the casing and the formation can also affect the instrument response. For example, materials like cement and bentonite, owing to the water retention capacity, can result in over estimates of water content relative to antecedent values. In addition to casing configuration, characteristics of the formation, such as bulk density, soil/rock type, thermal neutron cross section, type of fluid in the pore space, temperature, and pressure. In the petroleum industry, it is not unusual to use multiple corrections for borehole and formation effects

Borehole and formation corrections developed in the petroleum industry do not apply to unconsolidated partially saturated conditions typical of Hanford. Ideally, each casing configuration in which neutron measurements are made requires a separate calibration, but this is not always practical. One approach is to develop a single calibration for standard conditions and derive corrections for configurations different from the conditions at calibration. A combination of these two approaches was used to develop the Hanford Moisture Calibration Standards and to calibrate the interim cover hydroprobe.

1.2 Scope and Objectives

The objective of this study was to use the MCNP code to calibrate the Campbell Pacific Nuclear (CPN) DR503 hydroprobe for use in 2-in.-diameter carbon steel well access tubes at the interim barrier demonstration project. Geometrical representation of the Hanford Calibration Standards, access tubes, and CPN probe, including the ^{3}He detector and shield, were generated from the actual dimensions and used for input for MCNP. Applying the MCNP code allowed the neutron count rates to be theoretically determined for the different access-tube configurations in the physical models. Neutron counts measured in the shield (N_s), dry air (N_a), and physical models using 6- and 8-in.-diameter carbon steel casings were used for comparison with the theoretical N and CR values. Calibrations in the standard casing diameters and smaller 2-in. casings were used to develop a prediction function for different casing diameters.

The following sections describe the theory of the neutron probe response, the configuration of the calibration standards, and the MCNP simulations. The results of the simulations are then used to generate calibration functions based on N and CR for 2-in. carbon steel access tubes. Given the depth of the access tubes, we hypothesize that differences in soil mineralogy are insufficient to warrant the development of different calibration functions for different layers. Consequently, a single calibration function is developed and is assumed to apply to deeper soil horizons.

2.0 Materials and Methods

Monte Carlo-based numerical simulations were performed using a generalized geometry for DR 503 Hydroprobe (Rick McCain, personal communication) and soil elemental compositions from the Hanford Moisture Calibration Standards. Simulations were performed for 6-in. and 8-in. steel casings at moisture contents of 5, 11.9, and 19.7 percent for comparison with observations in the moisture standards. In addition, simulations were performed in air and pure water and at two additional moisture contents, 25 and 32 percent. Simulations were also conducted for a 2-in. steel casing in the moisture standards, air and water. Clean silica sand (SiO_2) at 32 percent pore volume was used in the simulations. The volume fractions of water were simulated by the pore volumes consisting of a combination of air and water. The physical models constructed at Hanford were not entirely clean sand but contained hydrated alumina (Engleman et al. 1995). This section describes the neutron moisture logging system, the theory of the response, the calibration models, and the numerical simulations used to develop the calibration relationship.

2.1 Description of the Neutron Hydroprobe

The neutron probe of interest is the Model 503DR Hydroprobe manufactured by CPN International, Inc. (Martinez, CA). This instrument is used to determine soil water content using the neutron moderation technique. A major advantage of this technique is that the same soil profile can be repeatedly monitored over any length of time, at any sampling interval, and at any sample depth provided access tubes are installed to the depth of interest. Figure 2.1 shows a schematic of the hydroprobe housing, including the display, controls, and shield box.

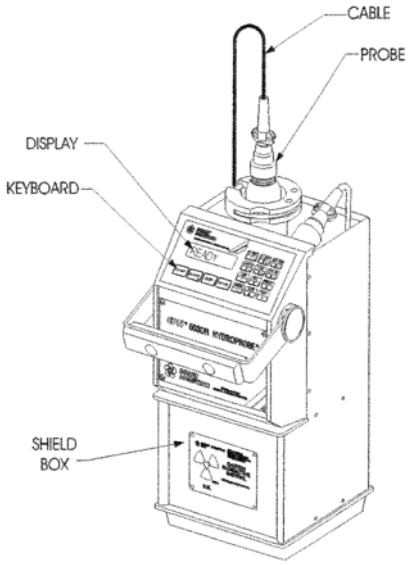

Figure 2.1. Schematic of a CPN 503DR Hydroprobe (after CPN, 1992)

Figure 2.2 shows a cross section of the hydroprobe (Rick McCain, personal Communication). This is a generalization only and details may actually vary between probes. The probe shell is constructed of aluminum tubing with an outer diameter (o.d.) of 1.5 inches, a wall thickness of 0.083 inches, and a

length of 12 inches. The detector used to measure thermalized neutrons is a ^{3}He-filled proportional counter housed in a 13.2-cm-long by 2.54-cm-diameter stainless steel cylinder (wall thickness 0.20 inches) at a pressure of 6 Atm. The detector is positioned vertically in the cylindrical probe housing, opposite the neutron source. The detector is surrounded by an inner layer of polyethylene (1.0 in. i.d., 1.334 in. o.d., and 1.25 in. long) and an outer layer of cadmium (0.01 cm thick). The cadmium absorbs low energy or thermal neutrons whereas the polyethylene moderator slows down epithermal or higher energy neutrons before they enter the detector to increase the efficiency of detection. The polyethylene moderator is limited to the sides of the detector and does not extend to the region between the detector and source so as to reduce the detection of direct source neutrons, which could add to the background signal. Fast neutrons are generated by a 50-mCi (1.85 GBq) ^{241}Am-Be source enclosed in a capsule 0.5 inches high with a diameter of 0.375 inches. The sources capsule is housed in a tungsten carbide enclosure. The neutron source is located approximately 3 cm below the detector. This geometry was used as the basis for the MCNP model configuration.

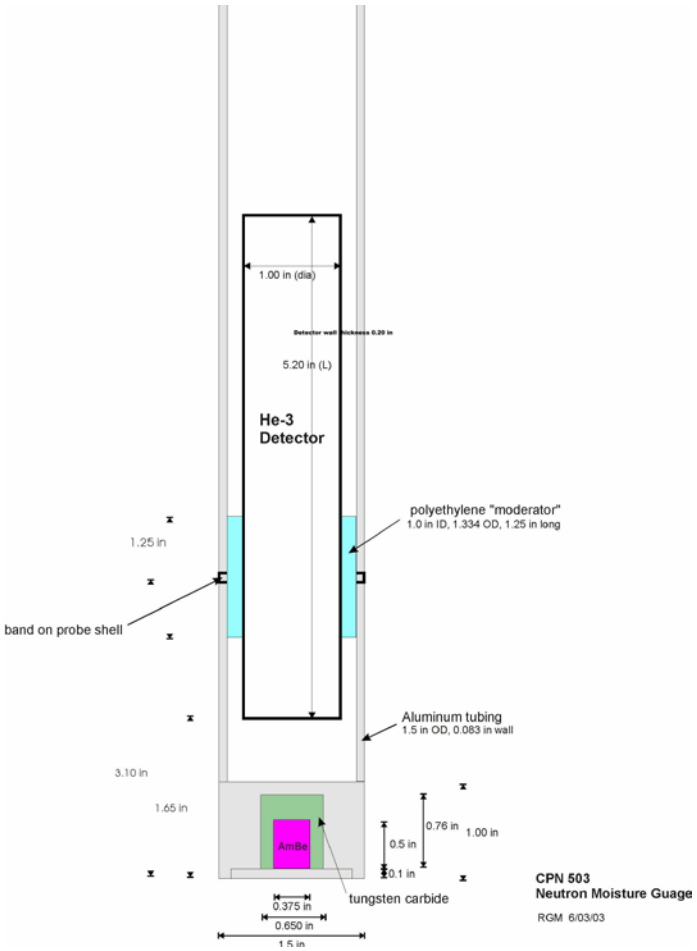

Figure 2.2. Generalized Cross-Sectional View of the Geometry Used in the MCNP Simulations of the DR 503 Neutron Probe Design (Rick McCain, personal communication)

Another important component of the hydroprobe that is important to the MCNP simulation is the configuration of the shield. The operator's manual for the CPN DR503 hydroprobe describes the shield as being composed of silicon-based paraffin (CPN 1992). However, there are no descriptions of the composition or molecular structure, information that is critical as input for the MCNP simulations of probe response. The exact molecular structure of the silicon-based paraffin used in the shield is not known. It is known that pure paraffin wax ($C_{25}H_{52}$) is a good electrical insulator and an effective neutron moderator, the efficiency of which is improved by adding silicon. The likely structure and properties were derived from the work of Lewis (1958). Lewis (1958) described dimethyl siloxane, $(CH_3)_3[OSi(CH_3)_2]_nOSi(CH_3)_3$, liquids with molecular structures similar to those of the straight-chain alkanes. The main skeleton consists of silicon-oxygen linkages rather than the carbon linkages of the straight-chain hydrocarbons, and methyl side groups are added at the silicon atoms. The main structural features of the silicone and *n*-paraffin molecules are illustrated in Figure 2.3. The main difference between the two structures is that whereas the skeleton is well shielded by hydrogen atoms in the *n*-paraffins, the siloxane skeleton is comparatively exposed at the oxygen sites. The length of the molecule is determined by n. For large *n*, the atom ratios are H = 0.6, Si = 0.10, C = 0.2, and O = 0.1. These ratios correspond to weight fractions of H = 0.10227, Si = 0.35622, C = 0.40623, and O = 0.13528. The value of *n* was unknown, but for the simulations was optimized by matching the measured and simulated shield counts for different values of *n*.

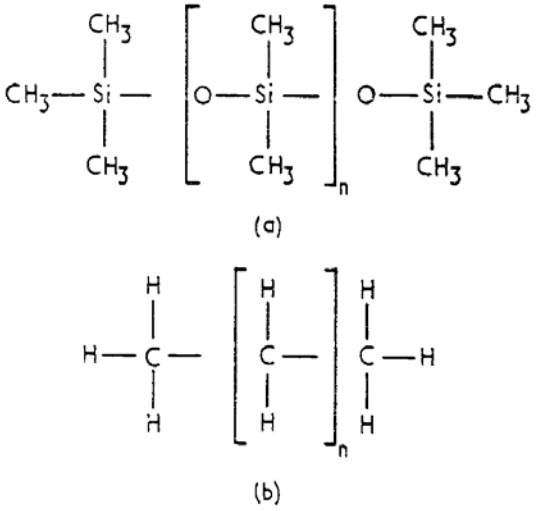

Figure 2.3. Structural Formulae for Silicone and n-Paraffin Molecules. The length of the molecule is determined by the integer *n* (after Lewis 1958).

Neutron measurements are widely used in agriculture, forestry, hydrology, and civil engineering to measure the water content of soil. Compared to the gravimetric method, the neutron method is fast and nondestructive, allowing repeated measurements to be made *in situ*. The neutron technique has proven to be a convenient and effective means for monitoring long-term *in situ* soil moisture variations but requires calibration to relate neutron counts to soil moisture contents.

Neutron probe measurements in unconsolidated materials require the use of an access tube. Apart from the initial installation of access tubes, the technique is essentially nondestructive. The neutron probe has an o.d. of 1.500 inches, and the manufacturer recommends an access tube with an i.d. of at least

1.555 inches. Access tubes are typically capped at the top to prevent water intrusion. Ideally, access tubes are constructed of aluminum, but they are often constructed of steel and even polyvinyl chloride. After making a shield reading, hydroprobe measurements are made by lowering the probe housing down an access tube. The probe is then withdrawn from the access tube, manually or by a winch, at a speed that allows a measurement at each depth of interest. Manual measurements typically involve pausing at the depth of interest to collect a 30-s count. Borehole logging with a winch system uses a predetermined logging speed such that the vertical spatial resolution is about 3 inches. The probe measures the number of thermalized neutrons, and this is often expressed as a ratio to the shield count to give a CR. The water content is typically regressed on CR to obtain the calibration function. The CR in natural soils is influenced by the moisture content, soil elemental composition, bulk density, and proximity of the probe to the water table and soil surface (Dickey 1990; Dickey and Schwankl 1980). Neutron counts are also influenced by the strength of the neutron source, the size and type of the neutron detector, the position of the detector relative to the source, and the size and type of access tube (Schmugge et al. 1980; Stone 1990).

2.1.1 Theory of Response

Understanding the theory of the hydroprobe response is essential for developing the correct conceptual model for the MCNP simulations that will be the basis of the calibration. The fundamental basis of the neutron method is the scattering of neutrons by elastic and non-elastic collisions with soil particles and hydrogen. The neutron source emits fast neutrons, which interact with soil particles and soil water that surrounds the probe (Figure 2.4). When the probe is lowered into the access tube, a stable, spherical "cloud" of slow neutrons develops around the source (Greacen et al. 1981; IAEA 1970). The radius of the sphere of influence accounting for 95% of the neutron flux that would be obtained in an infinite medium is given by Olgaard (1965) and Kristensen (1973) as

$$R = \frac{100}{1.4 + 0.1\theta} \tag{2.1}$$

where R is the radius (cm), and θ is the volumetric water content in (%)—thus, the drier the soil, the larger the radius of the sphere of influence.

The number of slow neutrons per unit volume in the sphere remains constant and is proportional to the water content of the soil within the sphere of influence. Since the slow neutron detector is placed inside the cloud volume, the CR (counts per minute [cpm] or cps) is proportional to the soil water content, θ, of the same volume. The instrument must therefore be calibrated with samples of known water content. The collision of fast neutrons (energy > 2 million electron volts [MeV]) with hydrogen and other atoms results in the moderation of the neutrons. They lose energy to become slow or thermal neutrons with energies < 0.025 electron volts (eV) (Figure 2.5). Since neutrons have no charge, the electric fields associated with the charged soil particles do not affect their movement. Neutron absorption by various nuclei depends on the energy of the neutron and the particular target nucleus. Li et al. (2003) showed that the average energy loss per collision, ξ, depends primarily on the atomic mass of the impacted nucleus and is independent of the initial energy of the neutrons. In other words, after each collision, the neutron always loses the same fraction of its energy. This fraction decreases with increasing atomic mass of the impacted nucleus (Li et al. 2003). Using ξ, Li et al. (2003) calculated the average number of collisions required to convert fast neutrons with the initial energy of E_0 (E_0 = 2 MeV) to the thermal values

(E = 0.025 eV). Table 2.1 summarizes the number of collisions required to thermalize a fast neutron for selected elements. Owing to the similarity in size between the neutron and the hydrogen atom, hydrogen is the most efficient target atom for reducing neutron energy. Hydrogen is therefore a good neutron moderator, and because hydrogen is a major constituent of water, water is also a good neutron moderator.

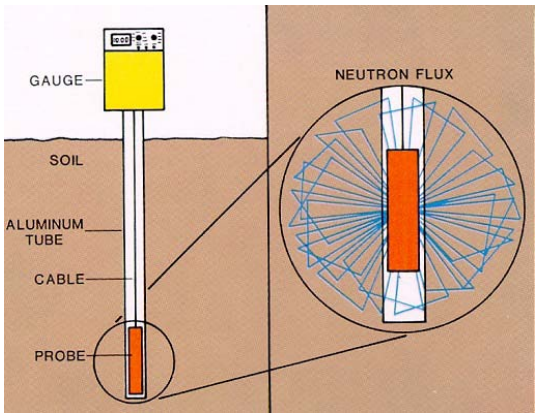

Figure 2.4. Schematic Depiction of Neutron Hydroprobe Deployment

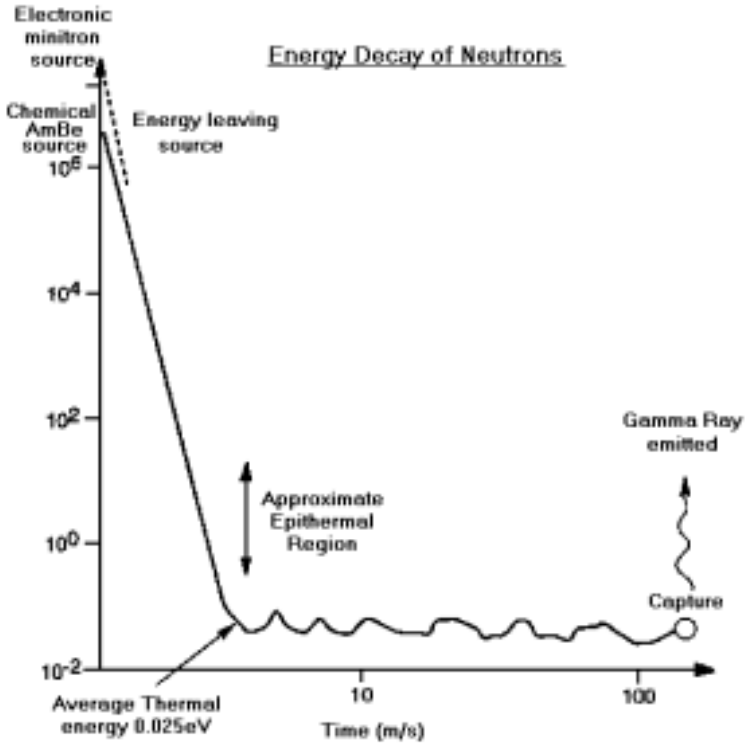

Figure 2.5. Energy Decay of Fast Neutrons

Table 2.1. Number of Elastic Collisions Necessary to Reduce the Energy of a Neutron from 4 MeV to 0.025 eV for Selected Elements

Target Isotope	Atomic Mass	ξ	Number of Collisions
Hydrogen	1.008	1.00000	18
Deuterium	2.000	0.72500	25
Helium	4.003	0.42500	43
Lithium	6.940	0.26200	69
Beryllium	9.013	0.20600	88
Carbon	12.011	0.15800	115
Oxygen	16.000	0.12000	152
Sodium	22.991	0.08500	215
Iron	22.850	0.35400	514
Uranium	238.070	0.00838	2,172

On the collision of a fast neutron with an atom having atomic number, A, (A=Z+N; where Z = atomic number, and N is the number of neutrons), one neutron is absorbed by a nucleus ${}^{A}_{Z}X$ according to:

$$ {}^{1}_{0}n + {}^{A}_{z}X \rightarrow {}^{A+1}_{z}X \tag{2.2}$$

The modified nucleus ${}^{A+1}_{Z}X$ may be unstable and disintegrates emitting gamma radiation (Figure 2.5). However, this occurs with only a few nuclei present in soils (e.g., Ag, Au, In, Fe, Al, and Mn) that are typically present at very low concentrations. Because the neutron flux emitted by the source is generally low in intensity, the probability of neutron capture is extremely low. In many cases, ${}^{A+1}_{Z}X$ is stable, and the reaction can be described by:

$$ {}^{12}_{6}C + {}^{1}_{0}n \rightarrow {}^{13}_{6}C;\ {}^{14}_{7}N + {}^{1}_{0}n \rightarrow {}^{15}_{7}N \tag{2.3}$$

The reaction can also lead to radioactive products, although the half-lives are typically very short. For example, with an aluminum access tube, the following reaction can occur:

$$ {}^{23}_{13}Al + {}^{1}_{0}n \rightarrow {}^{24}_{13}Al \tag{2.4}$$

The half-life of ${}^{24}_{13}Al$ is only 2.3 minutes, so any radioactivity that may develop in the aluminum access tubes during a measurement decays rather quickly. There is essentially no activation of soil material when a neutron probe is used. Free neutrons are unstable and disintegrate relatively quickly as $t_{1/2}$ is around 13 minutes. Thus, if a free neutron is not captured, it will quickly disintegrate according to:

$$ {}^{1}_{0}n \rightarrow {}^{1}_{1}p + \beta^{-} + \nu_{e} + 780\,KeV \tag{2.5}$$

with a release of 780 KeV of energy. In Equation (2.5), ${}^{1}_{1}p$ is a proton, β^- is a beta particle, and ν_e is a neutrino.

2.1.2 Source of Neutrons

The source of neutrons in the CPN Model 503DR Hydroprobe is americium-241 (^{241}Am) and beryllium. The ^{241}Am-Be source is typically permanently sealed in a shielded canister. With a half-life of approximately 460 years, the source can maintain a constant rate of production of fast neutrons for a very long time. Americium-241 is an unstable isotope with an excess of protons (Z/N = 95/146 = 0.65). It decays to neptunium with the liberation of an alpha (α) particle with 5.48 MeV of energy and a gamma-ray of 60 thousand electron volts (KeV), according to:

$$^{241}_{95}Am \rightarrow {}^{237}_{93}Np + {}^{4}_{2}\alpha + E \tag{2.6}$$

Compared to ^{241}Am, the resulting isotope of neptunium has a smaller excess of protons with a smaller Z/N ratio of 0.64. Neptunium is also unstable and subsequently undergoes decay. Beryllium, the other component of the source, contains an excess of neutrons (Z/N =0.8). Beryllium reacts with the α particles emitted from ^{241}Am and is converted into carbon, releasing ‘‘fast neutrons’’ in the process according to the reaction

$$^{9}_{4}Be + {}^{4}_{2}\alpha \rightarrow {}^{13}_{6}C \rightarrow {}^{12}_{6}C + {}^{1}_{0}n + E \tag{2.7}$$

Compared to $^{9}_{4}Be$, the new isotopes $^{12}_{6}C$ and $^{13}_{6}C$ have smaller excesses of neutrons with higher Z/N ratios (Z/N = 0.86 and Z/N = 1, respectively). The isotope $^{13}_{6}C$ is unstable and by emitting a fast neutron decays to $^{12}_{6}C$. Most neutron probes therefore emit a low level of γ radiation, which may arise from the radioisotope itself or from $^{12}_{6}C$ left in the excited state after conversion from beryllium (IAEA 1970). A major advantage of the ^{241}Am-Be source is the much lower level of γ radiation produced compared to other sources (e.g., ^{226}Ra-Be) and the corresponding lower shielding requirements.

2.1.3 Neutron Energy Spectrum

Information on the neutron energy spectrum is needed to simulate the response of the 503DR Hydroprobe. Neutron transport involves a spectrum of energy levels, scattering collisions, and absorption reactions. The energy spectra for ^{241}Am-Be sources are depicted in Figure 2.6. Fast neutrons generated by the ^{241}Am-Be source have a mean energy of around 4.5 MeV and a maximum energy of 11 MeV (IAEA 1970). Fast neutrons are defined here as those having kinetic energies in excess of 2 eV. As the fast neutrons diffuse in the soil medium, they are slowed down and lose energy, mainly by elastic collisions with hydrogen nuclei, and to a lesser extent by absorption, finally becoming thermalized. Slow neutrons are defined as those with kinetic energy less than 2 eV. Slow neutrons may be further divided into two groups: “thermal neutrons” having energies from 0 to 0.5 eV, and “epithermal neutrons” with energies between 0.5 and 2.0 eV (IAEA 1970).

Although it is well documented that hydroprobe has a 50mCi AmBe source, the actual strength is typically not well characterized strength. Because the count rate is controlled by a number of factors including absolute source strength and detector efficiency, accurate predictions of absolute counts often requires optimization of the source against a benchmark dataset . It is know that the neutron flux

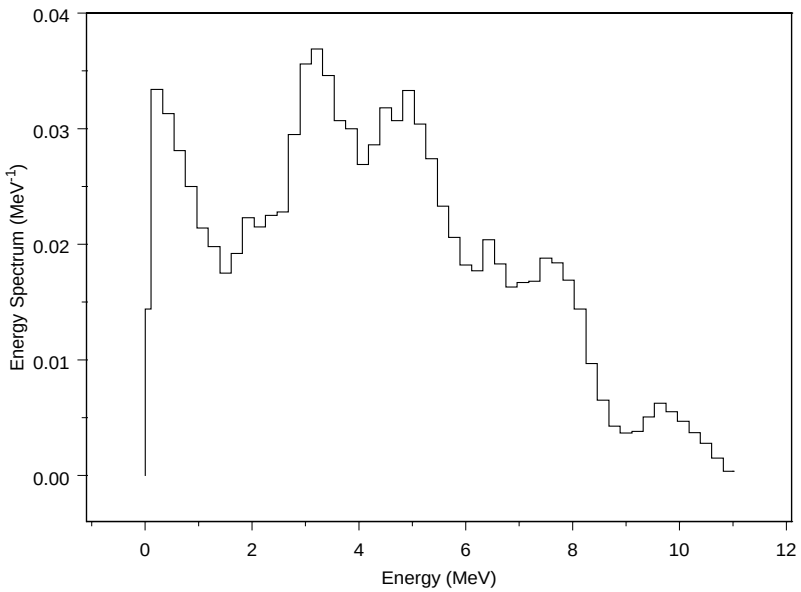

Figure 2.6. Neutron Energy Spectra for ^{241}Am-Be Isotopic Neutron Source as Defined by ISO 8529-1 (ISO 2001) Normalized to 1 mCi ^{241}Am

The source strength was optimized using the measurements made in the calibration models with 6-in. steel wells. Although the ISO Standard suggests a neutron flux of 111,000 neutrons (n) for a 50 mCi source (50 × 2220 n/s), it was not possible to match the absolute count rates measured in the calibration models with this flux. The source strength was optimized using the measurements made in the calibration models with 6-in. steel wells and shield. The result suggested a flux of 141,367 particles or 2,827 n/s which was used in of the MCNP simulations.

2.1.4 Detector

There are several slow neutron detectors available, but the one used in the CPN DR503 is a ^{3}He detector. The probe housing includes a slow neutron detector and a pre-amplifier. The detector is housed in a 2.54-cm-diameter by 28-cm-long sealed stainless steel cylinder with ^{3}He gas at 6 Atm of pressure. The ^{3}He gas absorbs slow neutrons returning to the sensor, after thermalization, according to the nuclear reaction:

$$^{3}He + n \rightarrow p + T + 765\,keV \tag{2.8}$$

The emitted photons are detected as electrical pulses with an electronic counting device. Each count therefore corresponds to an electrical pulse originating from one slow neutron reaching the detector. The pulses coming from the detector are first pre-amplified in the probe. The pre-amplified pulses are then transmitted to the electronic counting system through the cable that connects probe to the electronics. Electronic counting systems vary with probe type, but typically consist of an amplifier, a high-voltage source, a counter, a timer, rechargeable batteries, and a microprocessor. The number of thermalized neutrons is proportional to the soil water content in the sphere of influence. The microprocessor sums the returning thermalized neutrons over a 16-s sample time to provide a raw count in terms of cpm or cps. A CR is calculated as the quotient of the raw count to the shield count. Calibration functions can be derived

by substituting either the raw count value or the CR into the appropriate regression equation to predict volumetric water content.

2.2 Description of Calibration Standards

At Hanford, calibration relationships have been developed using physical models composed of mixtures of silica sand and hydrated alumina (Engleman et al. 1995). The moisture calibration models were designed to cover the Hanford moisture range and to have a bulk density representative of actual formations. Three moisture models with 6-in. and 8-in.-diameter steel access tubes are included in the Hanford Calibration Standards. The three models include water contents of 5, 11, and 20 volume percent (0.05, 0.11, and 0.20 $m^3\ m^{-3}$), respectively. These water contents were chosen after examining a database of over 3600 gravimetric moisture contents for Hanford Formation sediments (Engleman et al. 1995). These data showed that volumetric water content in the vadose zone typically ranges between 0.04 and 0.40 $m^3\ m^{-3}$, with a mode of 0.05 $m^3\ m^{-3}$. A smaller database of *ex situ* dry bulk density measurements (550 data points) showed a mean value of 1.81 g/cm^3, a median of 1.79 g/cm^3, and a mode of 1.70 g/cm^3.

The models are contained in seven cylindrical tanks, each with a steel casing along its axis for logging tool insertion (Figure 2.7). A complete description of the tank specifications is provided by Engleman et al. (1995). Briefly, each tank was constructed of 300 series (ASTM 24) 0.25-in.-thick stainless steel. The height of each tank is 1.9 m (inside) whereas the inside diameter is 1.5 m. Well casings were constructed of carbon steel (ASTM Schedule 40) and were of two sizes. Three of the models included casings with an i.d. of 6 in. (15.4 cm) and a wall thickness of 0.71 cm. The remaining four models were constructed with casings of 8 in. (20.3 cm) with a wall thickness of 0.82 cm. Accuracy of the casing thickness reported for the 6-in. and 8-in. casings is not known as the thickness of the 8-in. casing constructed into the moisture models was not measured at the time of construction. A thickness is 0.322 in. is assumed based upon the specification of schedule 40 carbon steel casing (tolerance quoted is ± 0.050 in.). Each tank was placed in a 1.8-m × 1.8-m × 0.2-m-high pallet constructed of 300 series (ASTM 240) stainless steel.

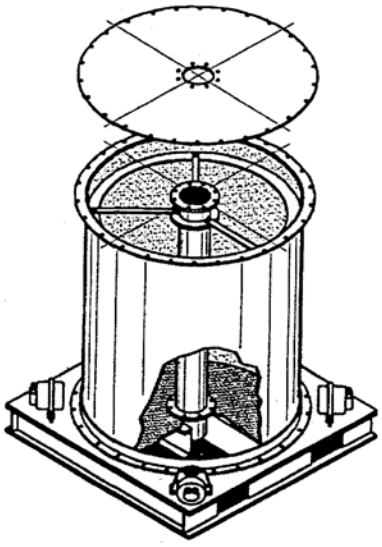

Figure 2.7. Schematic of Calibration Model (after Engleman et al. 1995)

The equivalent water content of each model was varied by varying the composition of dry, two-component mixtures of hydrated alumina, $Al_2O_3 \cdot 3H_2O$, and either SiO_2 or Al_2O_3. Al_2O_3. The hydrated alumina provides the hydrogen that emulates partially saturated sediments without the need to add water, which would tend to redistribute in the model. The water in $Al_2O_3 \cdot 3H_2O$ is chemically bound and maintains an even distribution in the model. Particle densities are needed as input for the MCNP simulations and were reported to be 2.42 g/cm^3 for hydrated alumina, 2.64 g/cm^3 for SiO_2, and 3.76 g/cm^3 for Al_2O_3 (Engleman et al. 1995). Six of the models contain uniform mixtures to achieve a specific equivalent water content, and one model contains a 102-cm-thick zone of 0.40 m^3m^{-3} between two 0.05 m^3m^{-3} moisture zones. The six homogenous models were vibrated to obtain desired bulk densities. The measured bulk density of the four 8-in. casing models is 1.76 g/cm^3, 1.76 g/cm^3, 1.70 g/cm^3, and 1.32 g/cm^3 for the 0.05 m^3m^{-3}, 0.1197 m^3m^{-3}, 0.197 m^3m^{-3}, and 0.409 m^3m^{-3} models, respectively. The seventh model with the high-moisture thin zone was not subjected to vibration packing so as to maintain a clear and level interface between the low moisture zones and the thin high moisture zone. This model, model D, is not used as a calibration standard for moisture content, but to study the thin bed response of the borehole tools.

Table 2.2 summarizes the configuration of the physical models, including casing diameter, equivalent water content, and bulk density. Detailed descriptions of the models, including weights of materials used in each model, are provided in the Appendix of Engleman et al. (1995).

Table 2.2. Configuration of Physical Models (After Engleman et al. 1995)

Model	Casing Outside Diameter (in.)	θ (m^3 m^{-3})	Bulk Density (kg m^{-3})
F	6	0.050	1760
E	6	0.118	1740
G	6	0.198	1700
A	8	0.050	1760
C	8	0.119	1760
B	8	0.197	1700
D-bottom	8	0.051	1560
D-middle	8	0.053	1630
D-top	8	0.409	1320

Each model provides three data points, 0.05 m^3m^{-3}, 0.12 m^3m^{-3}, and 0.20 m^3m^{-3}, which can be used to calibrate a neutron probe for two casing diameters, 6-in. and 8-in. In addition, a measurement is typically made in air and set equal to a water content of 0.0 m^3m^{-3}. Calibration functions based on these models have been developed and are routinely used onsite, but are inappropriate for determining water contents in access tubes other than 6- or 8-in.-diameter carbon steel access tubes or for formations wetter than 0.20 m^3 m^{-3}.

As part of the calibration process for the 2-in.-diameter steel casings, the MCNP model was first used to simulate the response of the neutron probe in the physical models, and the results were compared with actual measurements recorded by Stoller. The model was then used to simulate the response of neutron probes in a 2-in. steel casing.

2.3 Calculations Using the MCNP Computer Code

The MCNP neutron transport code was used to predict the responses of the neutron detector to changes in the configuration of the calibration model, including the diameter of the access tubes and the water content as inferred from the ratio of hydrated alumina to silica sand. The first step in preparing the simulations was to create geometric models representative of the probe and calibration models. The geometry of MCNP treats an arbitrary 3-D configuration of user-defined materials in geometric cells bounded by first- and second-degree surfaces in a Cartesian coordinate system (MCNP 2003). Usually, the geometry function, even for sources with complex geometries, is calculated according to point or line approximation. Cells are defined by the intersections, unions, and complements of the regions bounded by the surfaces (Briesmeister 2000). For the neutron probe and calibration model, surfaces were defined by supplying known points on the surfaces.

Figure 2.8 shows a schematic representation of the hydroprobe inside the calibration model, including the probe, well casing, and walls of the stainless steel tank as used in the MCNP model. Figure 2.9 shows the detailed geometry of the hydroprobe cross section as used in the MCNP model. Both schematics illustrate how surfaces are used to define cells. Each cell is bounded by a surface, multiple surfaces, or by infinity.

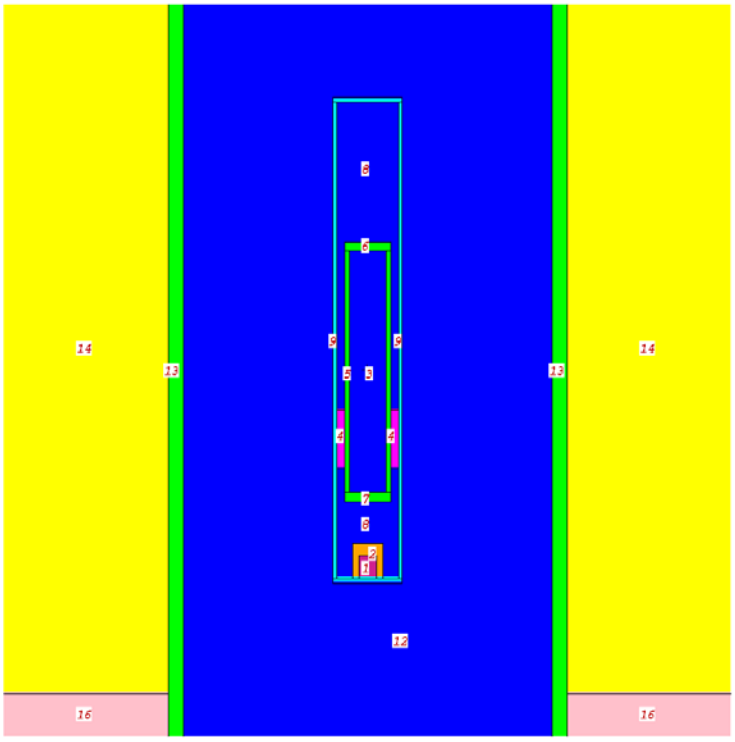

Figure 2.8. Detailed Configuration of the DR 503 CPN 503DR Hydroprobe Inside Calibration Model

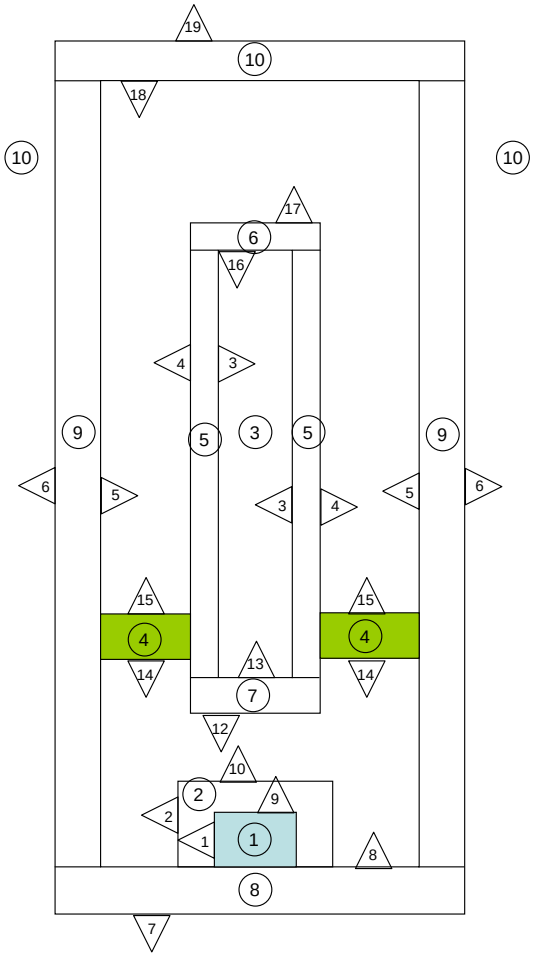

Figure 2.9. Detailed Configuration of DR 503 CPN 503DR Hydroprobe

Numbers in triangles are surface identification numbers whereas numbers in circles identify the cell. For example, the sensor housing in Figure 2.9 is bounded by a cylinder parallel to the z-axis (Cell 5) and two planes (Cells 6 and 7) perpendicular to the z-axis. The vertical cylinder (Cell 5) is bounded by an inner surface (surface 3) and an outer surface (surface 4). The upper plane is bounded by an inside surface (surface 16) and an outer surface (surface 17) whereas the lower plane is bounded by an inside surface (surface 13) and an outer surface (surface 12). Similarly, the outer housing of the probe is bounded by a vertical cylinder (cell 9) with an inner surface (#5) and an outer surface (#6) and two horizontal planes. The upper horizontal plane (Cell 10) is bounded by inner and outer surfaces, 18 and 19, respectively. The lower horizontal plane (Cell 8) is bounded by inner and outer surfaces, 8 and 7, respectively. There can be no gaps in the geometry, i.e., there can be no points that are not associated with a cell or surface. Specific problem geometries are developed by defining cells that are bounded by one or more surfaces. Cells can be filled with a specific material or defined as a void.

With the problem surfaces defined, the next step was to specify the materials, their physical properties, the physics of the radiation transport problem, and specifics for scoring the results (tallies) for the MCNP calculation. Material properties for the probe and calibration model components were obtained from the compendium of material composition data (Williams et al. 2006). Neutron reactions and cross-section specifications were derived from the ENDF/B-VI. In all instances, cross sections were

available for elements with naturally occurring abundances. The weight fractions of Am and Be in the ^{241}Am-Be source were calculated assuming a ratio of 13 $^{9}_{4}Be$ atoms to each $^{241}_{95}Am$ atom.

The sand used in the simulations was assumed to be composed of 10 elements, Si, Fe, Ca, Mg, O, Na, K, C, and Mn, with weight fractions according to Table 2.3. Table 2.4 presents a summary of the composition of the different calibration models. Table 2.5 is a summary of the elemental composition of the porous medium used in each calibration model, taking into account the change in the chemically bound water.

Table 2.3. Elemental Composition of Silicaceous Sand

Element	Mass (%)
H	3.760
C	5.936
O	44.144
Si	34.560
Al	0.940
Fe	2.381
Ca	4.494
K	0.083
Na	0.075
Mg	3.627

Table 2.4. Elemental Composition of Silicaceous Sand

		Composition (%)		
Model	θ (m^3 m^{-3})	$Al(OH)_3$	Al_2O_3	Sand
A	5%	6.20	0.00	92.00
B	20%	33.58	0.00	66.00
C	12%	19.51	0.00	80.49
E	12%	19.51	0.00	80.49
F	5%	8.20	0.00	91.80
G	20%	33.58	0.00	66.42
D_{top}	5%	9.43	0.0000%	90.57
D_{mid}	40%	89.57	10.4300%	0.00
D_{bot}	5%	9.43	0.0000%	90.57

Table 2.5. Elemental Composition of Calibration Models Used as Input to the MCNP Materials Card

		$Al(OH)_3$			Al_2O_3		Silicaceous Sand								
Model	WC	Al	O	H	Al	O	Si	Fe	Ca	Mg	O	Na	K	C	Mn	Total
A	5%	0.0214	0.0382	0.0024	0.0000	0.0000	0.3075	0.0178	0.0764	0.0118	0.4627	0.0064	0.0124	0.0230	0.0007	0.981
B	20%	0.1159	0.2069	0.0129	0.0000	0.0000	0.2225	0.0129	0.0553	0.0085	0.3348	0.0046	0.0090	0.0166	0.0005	1.000
C	12%	0.0674	0.1202	0.0075	0.0000	0.0000	0.2696	0.0156	0.0670	0.0103	0.4057	0.0056	0.0109	0.0201	0.0006	1.000
E	12%	0.0674	0.1202	0.0075	0.0000	0.0000	0.2696	0.0156	0.0670	0.0103	0.4057	0.0056	0.0109	0.0201	0.0006	1.000
F	5%	0.0283	0.0505	0.0032	0.0000	0.0000	0.3075	0.0178	0.0764	0.0118	0.4627	0.0064	0.0124	0.0230	0.0007	1.000
G	20%	0.1159	0.2069	0.0129	0.0000	0.0000	0.2225	0.0129	0.0553	0.0085	0.3348	0.0046	0.0090	0.0166	0.0005	1.000
D_{top}	5%	0.0326	0.0581	0.0036	0.0000	0.0000	0.3034	0.0176	0.0754	0.0116	0.4565	0.0063	0.0122	0.0226	0.0007	1.000
D_{mid}	40%	0.3092	0.5520	0.0345	0.0551	0.0492	0.0000	0.0000	0.0000	0.0000	0.0000	0.0000	0.0000	0.0000	0.0000	1.000
D_{bot}	5%	0.0326	0.0581	0.0036	0.0000	0.0000	0.3034	0.0176	0.0754	0.0116	0.4565	0.0063	0.0122	0.0226	0.0007	1.000

Air filling the void in the probe housing was assumed to be air at sea level and atmospheric pressure. For the simulation of measurements in air ($\theta = 0.0$ m^3m^{-3}), the composition included H, C, N, O, and Ar, and the relative humidity varied from 0 to 100% to quantify the effects of humidity. The composition air, in terms of weight fractions and as a function of humidity, was derived from the work of Rivard et al. (2004). For the air simulations, the tank of the calibration model was removed, and the probe was assumed to be suspended in air. Simulations of the probe response in the shield were also run to provide a shield count for calculating the CRs.

The MCNP input file is used to describe the geometry of the problem, specify materials and radiation sources, and format the types of results needed from the calculation. Specific problem geometries were developed by defining cells that are bounded by one or more surfaces as described above. All simulations were run with a computing cutoff time of 1200 minutes. Example input files for the shield, air, and calibration model are attached as Appendices.

2.4 Calibration Procedure

Calibrating a neutron probe consists in quantifying the relation between neutron counts N in cps or the CR to volumetric soil water content, θ. Typically, a given soil is sampled over a range of θ while measuring N. In this study, the measured range of water contents corresponded to the water contents in the calibration models. This limited the calibration data to three values, namely 0.05, 0.12, and 0.20 m^3 m^{-3}, along with an air count rate, N_a, that was assigned a water content of 0 m^3 m^{-3}. In addition to these measurements, N was simulated for a medium with $\theta = 0.40$ m^3 m^{-3} and one with $\theta = 1.0$ m^3 m^{-3}, i.e. pure water. The calibration models were logged by Stoller using a 16-s count and sextuplicate counts for each model; the air and shield were also recorded.

Volumetric moisture content is then related to N or CR by

$$\theta = e^A \cdot f^B \tag{2.9}$$

where θ = volumetric water content
f = Count rate (N) or count ratio (CR)
A = empirical constant
B = empirical constant.

Equation (2.9) can be transformed to a linear equation as follows:

$$\ln(\theta) = A + B \times \ln(f) \tag{2.10}$$

For calibration, the counts, N_s, were measured in a standard (in this case, the shield), in air (N_a) and in the "soil" or calibration model, N. The raw count N was then used to calculate the CR as

$$CR = \frac{N}{N_s} = \frac{C \cdot T^{-1}}{C_s \cdot T^{-1}} \tag{2.11}$$

where C is neutron counts measured in the soil over time T (seconds, C_s, is the neutron counts measured in the standard over time, T_s (seconds), N the count rate in the soil or calibration model (cps), and N_s the count rate in the standard (cps). Either N or CR may be used as the independent variable in the regression with the known water contents as the dependent variable. Therefore, calibration functions will be developed from both variables. Equation (2.9) is the most practical formulation as it is usually desirable to predict θ from N or CR.

3.0 Results

Neutron-probe measurements were made in air, in three calibration models (E, F, G), and in the shield by Stoller using probe DR-503, serial number H370608792. For each measurement in the calibration model, the probe was placed at the center of the model and six 16-s-long measurements were made simultaneously. Any variation in the total counts at a fixed location is attributed to statistical phenomena. Making six measurements allows any systematic effects associated with the detector or electronics to be evaluated, such as gain shift. The MCNP model was calibrated using neutron counts made in the probe shield, air, and all of the physical models with 6-in. and 8-in. access tubes. The model was then used to predict the response in the 2-in. access tube

3.1 Calibration Measurements

Table 3.1 shows results of the calibration data for the 6-in. wells and includes measurements made in the shield, air and the calibration models. As can be expected, the lowest count occurred in air and the highest occurred in the shield. The average systematic error in N_a was 7.23% (one standard deviation) equivalent to a standard error of 1.28. The average systematic error in N_s determined from measurements in the shield was 1.34% (one standard deviation), equivalent to a standard error of 33.64. Table 3.2 shows results of the calibration data for the 8-in. wells and includes measurements made in the shield, air and the calibration models. The air measurements are the same as used for the 6-in model. This is because the air measurements are not made in an access tube but with the probe suspended in air (Rick McCain, personal communication). Measured N_a shows the highest average systematic error. Atmospheric conditions controlling the properties of air, particularity temperature and relative humidity, are quite variable, making N_a a poor choice for a standard. It is important that the standard count be taken under the same conditions, to the extent possible, as those used to establish the calibration. Moreover, it is important that the conditions be the same for each set of measurements.

In contrast, the average systematic error in the shield measurements, N_s, is quite small. The mean 16-s N_s associated with the 6-in. well calibration is 6168 with an average systematic error of 1.34 % (one standard deviation), equivalent to a standard error of 33. The mean N_s associated with 8-in. calibration measurements is 7335 with an average systematic error of 0.52% (one standard deviation), equivalent to a standard error of 16. The most striking observation is the discrepancy in N_s for the two datasets. The configuration used for the shield measurements in this study is not known. However it is known that the silicon-based paraffin in the shield has a finite volume an as such the shield is not 100% effective. Thus, the standard count can be impacted by surrounding conditions such as surface moisture and nearby objects. Nonetheless, the low systematic error in N_s and fact that it differs by around 16% between the 6-in. and 8-in. calibration measurements that may have been made under difference conditions supports its use as the standard for this analysis.

Figure 3.2 shows measured $\theta(N)$ for the 6-in. wells in the calibration models. The relationship between $\theta(CR)$ relationship is shown in Figure 3.2. The model parameters, fitted to Equation 2.9, and the associated standard errors are summarized in Table 3.3.

Table 3.1. Calibration Model Configuration and Experimental Measurements for 6-in. Wells

Medium	cps	Water Content (%)	θ (m^3m^{-3})	Mean cps	Standard Error, ε	CR
Shield	6204					
Shield	6213					
Shield	6174			6168.33	33.64	1.0000
Shield	6017					
Shield	6254					
shield	6148					
Model G	2832	19.80				
Model G	2825	19.80				
Model G	2955	19.80	0.198	2887.00	22.74	0.4680
Model G	2947	19.80				
Model G	2868	19.80				
Model G	2895	19.80				
Model E	2272	11.70				
Model E	2286	11.70				
Model E	2268	11.70	0.117	2264.00	17.44	0.3670
Model E	2196	11.70				
Model E	2322	11.70				
Model E	2240	11.70				
Model F	1524	5.00				
Model F	1605	5.00				
Model F	1514	5.00	0.05	1515.67	20.92	0.2457
Model F	1458	5.00				
Model F	1474	5.00				
Model F	1519	5.00				
Air	49	0.00				
Air	40	0.00				
Air	44	0.00	0.000	43.50	1.28	0.0071
Air	44	0.00				
Air	43	0.00				
Air	41	0.00				

Table 3.2. Calibration Model Configuration and Experimental Measurements for 8-in. Wells

Medium	cps	Water Content (%)	θ (m^3m^{-3})	Mean cps	Standard Error, ε	CR
Shield	7299					
Shield	7373					
Shield	7335			7335.64	15.70	1.0000
Shield	7349					
Shield	7375					
shield	7282					
Model B	2229	19.80				
Model B	2252	19.80				
Model B	2206	19.80	0.198	2236.69	7.05	0.3049
Model B	2239	19.80				
Model B	2242	19.80				
Model B	2251	19.80				
Model C	1824	11.70				
Model C	1845	11.70				
Model C	1849	11.70	0.117	1842.07	6.95	0.2511
Model C	1851	11.70				
Model C	1819	11.70				
Model C	1864	11.70				
Model A	1307	5.00				
Model A	1298	5.00				
Model A	1303	5.00	0.05	1295.12	4.11	0.1766
Model A	1278	5.00				
Model A	1292	5.00				
Model A	1292	5.00				
Air	49	0.00				
Air	40	0.00				
Air	44	0.00	0.000	43.50	1.28	0.0071
Air	44	0.00				
Air	43	0.00				
Air	41	0.00				

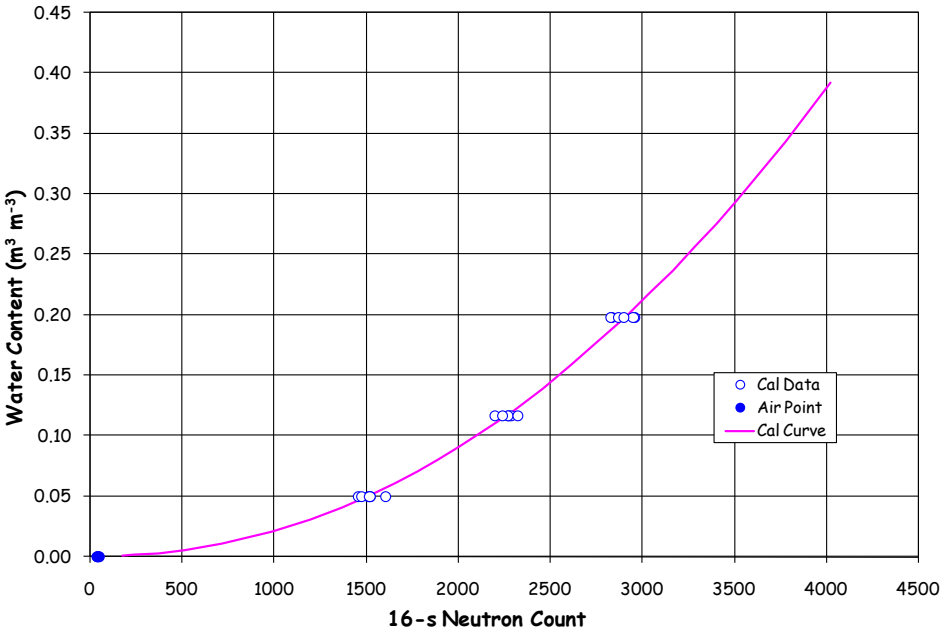

Figure 3.1. Measured Water Content as a Function of N in 6-in. Well Calibration Models

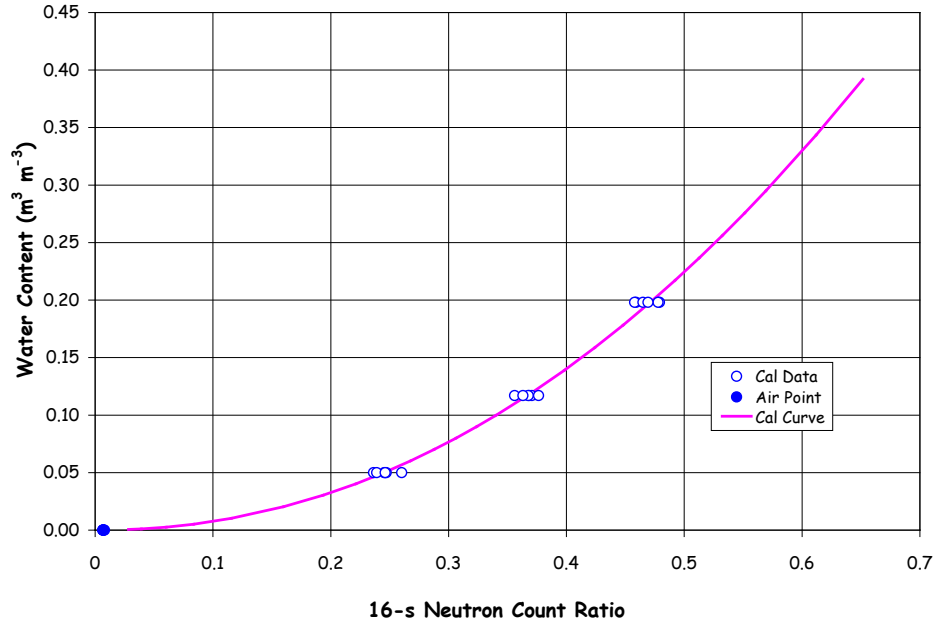

Figure 3.2. Measured Water Content as a Function of CR in 6-in. Well Calibration Models

Table 3.3. Fitted Model Parameters for Calibration Measurements in 6-in. Wells

Model	Equation	A	ε(A)	B	ε (B)
1	$\theta(N) = e^{A} \cdot N^{B}$	-18.4129	0.3582	2.1059	0.0468
2	$\theta(CR) = e^{A} \cdot CR^{B}$	-0.0343	0.0516	2.1059	0.0468

θ = volumetric water content (m^3m^{-3}); N = 16-s neutron count ; CR = 16-s neutron CR

Figure 3.3 shows measured θ(N) for the 8-in. wells in the calibration models. The relationship between θ(CR) relationship is shown in Figure 3.3. The model parameters, fitted to Equation 2.9, and the associated standard errors are summarized in Table 3.4. These parameters, when appropriately transformed, are essentially equal to those derived by Stoller Inc for converting N to the pore volume fraction or water content expressed as a percentage.

3.2 Calibration of MCNP Model

Successful prediction of the hydroprobe response for various probe, soil, and access tube configurations requires calibrating the MCNP model. Simulations were run with the MCNP code to predict the probe response in shield, in air, and in the calibration models with the 6-in. and 8-in. access tubes. The results of these simulations are summarized in the flowing sections.

3.2.1 MCNP Simulations of Shield Measurements

The shield count, N_s, is typically used as a standard count to normalize raw counts, N, and thereby calculate the CR. Thus, an accurate simulation of N_s is important to developing a robust calibration. However, simulating shield count is not straight forward as it depends to some extent on environmental conditions but more importantly because the exact structure of the silicon–based paraffin comprising the shield is not known. Owing to the uncertainty in the structure of the silicon–based paraffin, the first step was to optimize N_s by varying the properties of the shield. Properties were varied by changing the length, *n*, of the $(CH_3)_3[OSi(CH_3)_2]_nOSi(CH_3)_3$ molecule and the bulk density, ρ_b, as neither *n* nor ρ_b were known. The resulting parametric tests showed that the raw shield counts were sensitive to both n and ρ_b.

Increasing *n* from 3 to 100 showed an increase in N with increasing *n* with N increasing from around 8000 to around 8491 counts. For large values of *n*, the atomic ratios of $(CH_3)_3[OSi(CH_3)_2]_nOSi(CH_3)_3$ became constant at H=0.6, Si=0.10, C=0.2, and O=0.1, and increasing *n* did not have a significant effect on the simulated counts. This atomic ratio was therefore selected for all shield simulations. The next step was to optimize the ρ_b of the shield. Published values of ρ_b for paraffin range from as low as 0.76 g/cm^3 to 1.5 g/cm^3. Parametric tests between these two extremes showed N to be sensitive to ρ_b with N increasing as ρ_b increased. For example, the CR increased from 4733 cps at 0.76 g/cm^3 to 14953 at 1.5 g/cm^3. Nonlinear regression analysis showed that a shield ρ_b of 0.90 g/cm^3 provided the best match (6168.72 cps) with the field measurement of 6168.3 cps. A density of 0.90 g/cm^3 is slightly lower than the 0.93 g/cm^3 recommended for paraffin wax (William et al. 2006).

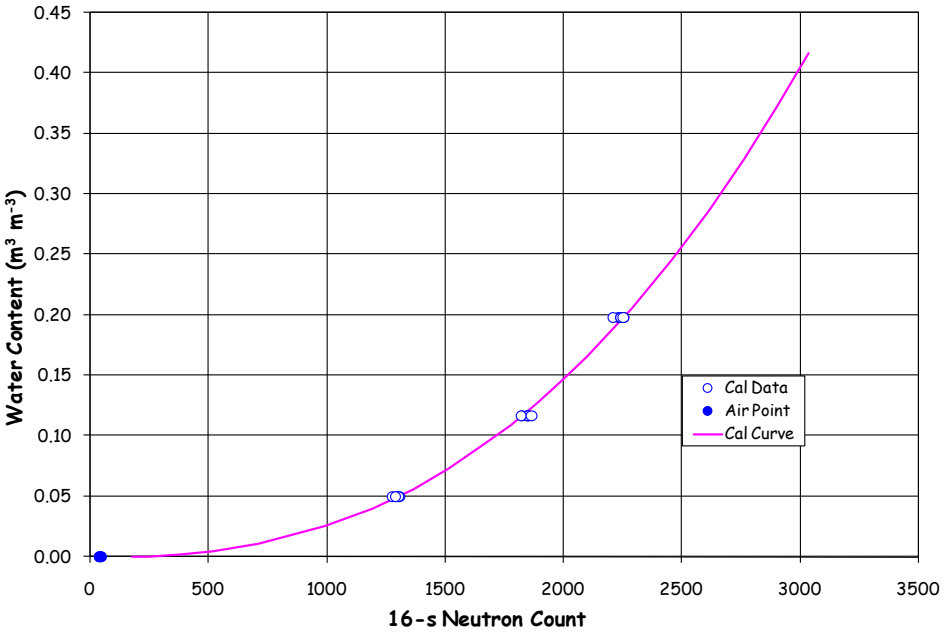

Figure 3.3. Measured Water Content as a Function of N in 8-in. Well Calibration Models

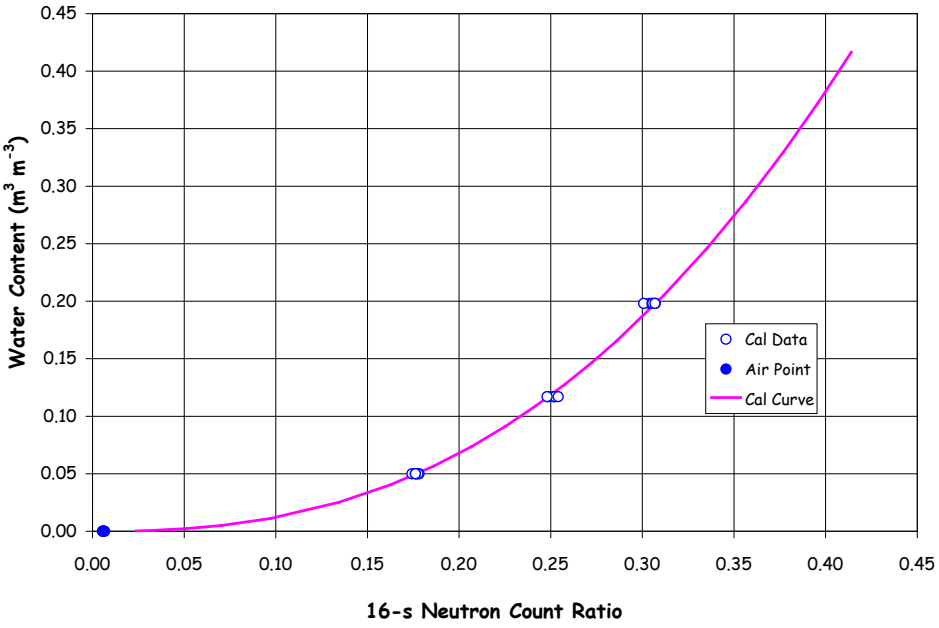

Figure 3.4. Measured Water Content as a Function of CR in 8-in. Well Calibration Models

Table 3.4. Fitted Model Parameters for Calibration Measurements in 8-in. Wells

Model	Equation	A	ε(A)	B	ε (B)
1	$\theta(N) = e^{A} \cdot N^{B}$	-20.889	0.2194	2.4958	0.0294
2	$\theta(CR) = e^{A} \cdot CR^{B}$	1.3254	0.0431	2.4986	0.0294

θ = volumetric water content (m^3m^{-3}); N = 16-s neutron count ; CR = 16-s neutron CR

Matching N_s for one data set does not guarantee a match for another dataset. As mentioned, the shield is not 100% effective so N_s is subject to surrounding conditions such as surface moisture and nearby objects. Therefore, use of N_s as a standard requires that it be measured under identical conditions. The CPN user's guide recommends measuring N_s by placing the gauge on the CPN nameplate depression on top of the case with the case on the ground. However, it is important that no other radioactive sources should be within 30 ft of the gauge, and no source of hydrogen should be within 10 ft after starting the reading.

3.2.2 MCNP Simulations of Air Measurements

The moisture content of air is controlled by the relative humidity, so neutron counts would be expected to vary with relative humidity. The composition of air (weight fraction) as a function of relative humidity at atmospheric pressure (101,325 kPa) is summarized in Table 3.5. The 24 tallies from the MCNP output, which is essentially equal to the number of neutrons per second per cubic centimeter of the detector volume, was converted to neutron cps by multiplying by 16 s × 42.8326 cm^3 (detector volume). The 24 tallies and the resulting neutron counts are also shown in Table 3.5.

These results show the CR to be relatively insensitive to the relative humidity of the air. The mean value of the counts (14.42 ± 0.085) simulated in air is significantly lower than mean value of 43.50 ± 7.23 cps reported by Stoller in their calibration measurements. This discrepancy could be a reflection of differences between the conceptual model for the air calibration and the field measurements. The MCNP simulations assumed the probe to be suspended in an air-filled cylinder 50 cm tall and 2 m in diameter surrounded by a void. It is likely that in the field, a probe suspended in air would be impacted by the soil surface below the probe. However, the exact conditions under which the air measurements were made in the field are not known, and matching the field measurements would require simulating the conditions used to establish the calibration.

Table 3.5. Composition (Weight Fraction) of Air as a function of Relative Humidity at Atmospheric Pressure and Simulated Neutron Counts

Relative Humidity (%)	Hydrogen	Carbon	Nitrogen	Oxygen	Argon	Tally 24 (× 10^{-2})	16-s Neutron Counts
0	0.00000	0.000124	0.755268	0.231781	0.012827	2.0909	14.32939
10	0.000181	0.000124	0.754048	0.232841	0.012806	2.1136	14.48496
40	0.000732	0.000123	0.750325	0.236077	0.012743	2.1134	14.48359
60	0.001101	0.000123	0.747837	0.238238	0.012701	2.1132	14.48222
100	0.001842	0.000122	0.742835	0.242585	0.012616	2.0907	14.32802

3.2.3 MCNP Simulations of Calibration Models

The MCNP model was then used to simulate the measurements made in six of the seven calibration models (Table 2.2), for the 6-in. and 8-in. steel cased wells. For the MCNP predictions all six calibration models were assumed to have the same size of well casing (either 6 in. or 8 in.) for a given set of simulations. No simulations were done for Model D with the thin bed. As shown in Table 3.1 and Table 3.2, calibration measurements were made in only six calibration models, namely models E, F, and G (6-in. steel wells) and in models A, B, and C (8-in steel wells).

3.2.3.1 Simulations with 6-in. Wells

Table 3.6 summarizes the results of the MCNP simulations of N in the three models assuming 6-in. wells. **Error! Reference source not found.** compares the MCNP simulated results to those obtained from the calibration models and includes the resulting calibration curve. Owing to the discrepancy in N_s measured in the 6-in and 8-in wells, we chose to optimize N_s for the 6-in well. This was accomplished by scaling the source strength to match the shield and calibration model readings. The result is a good match between the MCNP-predicted (6168.72) and measured (6168.33) N_s. As discussed before the discrepancy between the measured and predicted N_a is likely due to differences in the problem geometry. In general the MCNP-predicted N and CRs are in good agreement with the measured values showing differences of less than 1 percent. **Error! Reference source not found.** shows the regression of the MCNP-predicted on the field-measured N, both with a 16-s count time. Again, there is very good agreement with a relationship best described by a linear function with zero intercept, a slope of 1.002, and a coefficient of variation (r^2) of 0.999. Figure 3.7 shows a similar relationship of the MCNP-predicted CR values regressed on measured CR. The relationship is also linear with zero intercept, a slope of 1.001, and a coefficient of variation (r^2) of 0.999.

Table 3.6. Simulated Neutron Counts for the Calibration Models With a 6-in. Steel-Cased Well

Model	θ (m^3 m^{-3})	Bulk Density (kg m^{-3})	Measured 16-s N	Measured CR	MCNP 16-s N	MCNP CR
Shield	0.000	0.900	6168.33	1.0000	6168.72	1.0000
Air	0.000	1.205	43.50	0.0071	14.43	0.0023
F	0.050	1760	1515.67	0.2457	1515.59	0.2457
E	0.119	1740	2264.00	0.3670	2370.39	0.3843
G	0.197	1700	2887.00	0.4680	2840.45	0.4605
Water	1.000	997.1	NA	NA	4032.23	0.6537

3.2.3.2 Simulations with 8-in. Wells

Table 3.7 summarizes the results of the MCNP simulations of N in the three models with 8-in. wells. The most striking observation is that the predicted N_s is 16% smaller the measured value. The shield count is sensitive to environmental conditions at the time of measurement so it essentially impossible to simulate two shield counts obtained at different times outside a controlled environment. Stone et al (1995) examined effects of temperature, minor change of position of probe in shield, and stability of hydrogenous calibration media over time. Temperature was found to change count rates by an average of

-1.15 counts per minute per °C. Changes as small as 1 mm in the position of a probe in its shield were detectable in the shield count rate. If these conditions remain unchanged over the period of measurement

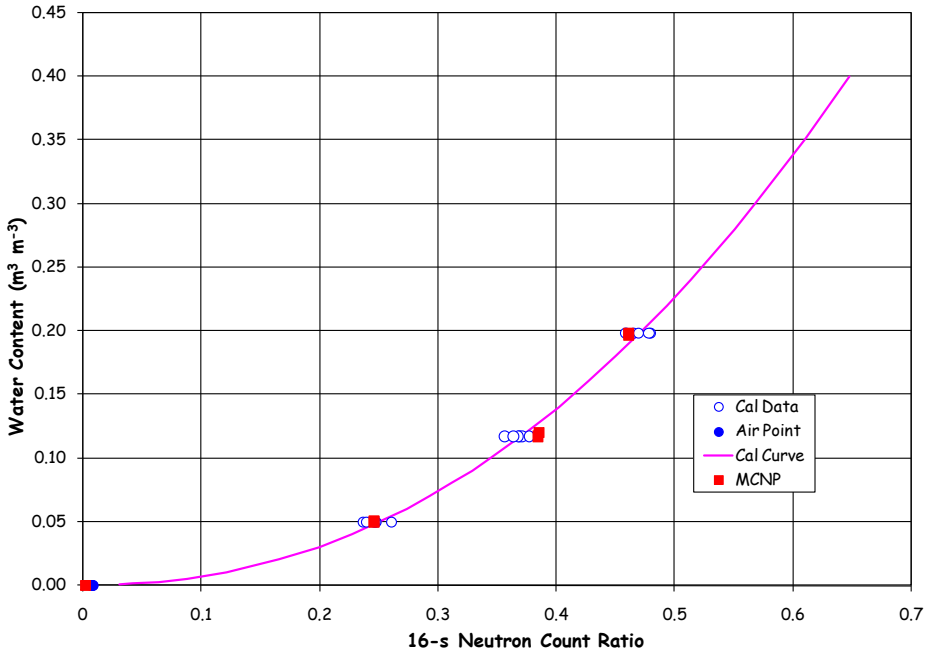

Figure 3.5. Water Content vs. MCNP-Predicted CR in a 6-in. Well

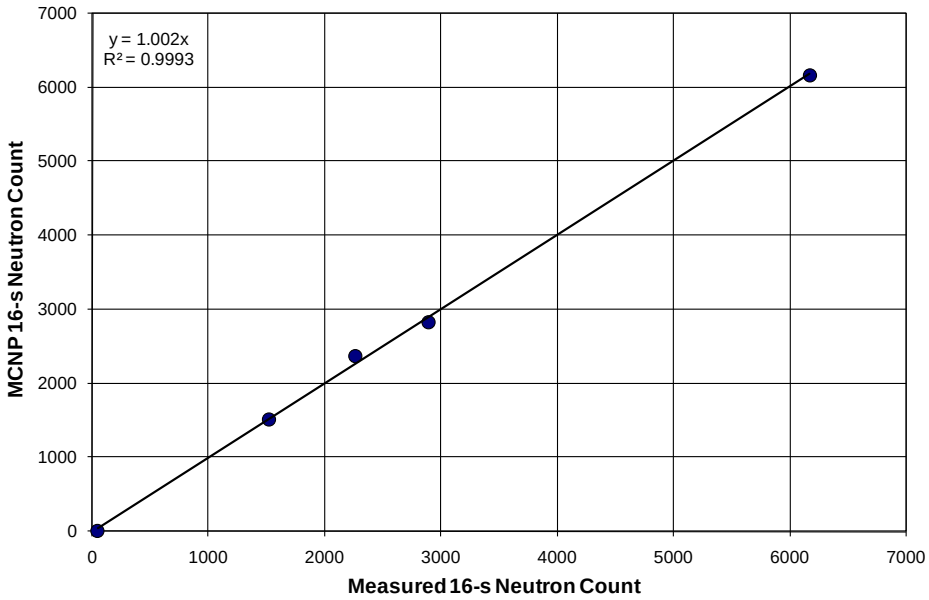

Figure 3.6. Relationship Between MCNP-predicted and Measured N in 6-in. Well

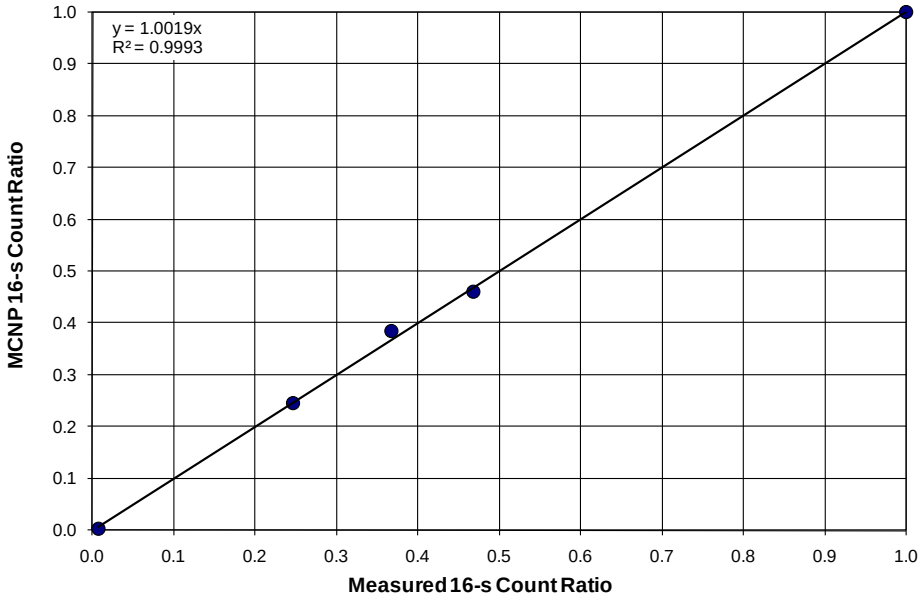

Figure 3.7. Relationship Between MCNP-predicted and Measured CR in 6-in. Well

Table 3.7. Simulated Neutron Counts for the Calibration Models With an 8-in. Steel-Cased Well

Model	θ (m^3 m^{-3})	Bulk Density (kg m^{-3})	Measured 16-s N	Measured CR	MCNP 16-s N	MCNP CR
Shield	0.000	0.900	7335.64	1.0000	6168.72	1.0000
Air	0.000	1.205	43.50	0.0059	14.43	0.0023
A	0.050	1760	1295.12	0.1766	1049.43	0.1701
B	0.197	1700	2236.69	0.3049	1839.54	0.2982
C	0.119	1760	1842.07	0.2511	1573.09	0.2550
Water	1.000	997.1	NA	NA	2457.91	0.3984

(verified by a shield count pre- and post-measurement) then a CR using the shield count would normalize N and minimize the effects of surrounding conditions. If the shield is used as a standard, each probe, even those of the same type, has to be calibrated because the shields are not identical (Hodnett and Bell. 1991).

Figure 3.9 compares the MCNP-predicted N to those obtained from the calibration models with 8-in. wells. The existing calibration curve for the 8-in data is also shown. The relatively poor match between the predicted and observed results can be expected given the discrepancy between N_s in the 6-in. wells and the 8-0in. wells. As expected the agreement between the MCNP-predicted N_s (6168.72) and the measured N_s (7323.61) is not as good as with the 6-in. results. The observed discrepancy is due primarily to differences in the conditions at the time of measurement and perhaps to differences in the geometry of the shield measurement. With the model, it is physically impossible to simultaneously match the absolute counts from two sets of conditions and geometries with a source strength optimized for one set of

conditions. The shield response is impacted by conditions surrounding the probe like temperature and even the position of the probe within the shield.

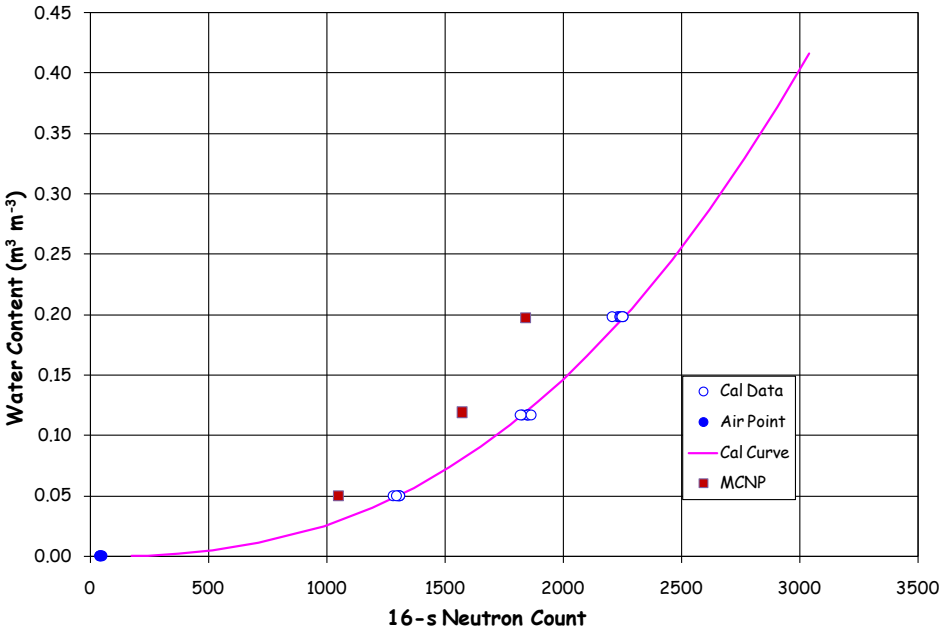

Figure 3.8. Water Content vs. MCNP-Predicted N in an 8-in. Well

Figure 3.9 shows the regression of the MCNP-predicted N on measured values. MCNP underestimates N over the range of values observed in the calibration. The relationship is linear with zero intercept, a slope of 0.8405 and a coefficient of determination (r^2) of 0.9998. Normalizing the predicted N with N_s to get CRs should narrow the discrepancy. In fact the MCNP-predicted CRs are in good agreement with the measured values showing differences of less than 1 percent (Table 3.7). Figure 3.9 compares the MCNP-predicted CR to those obtained from the calibration models with 8-in. wells. The resulting calibration curves for the 8-in data is also shown and is a marked improvement over that derived from the absolute values of N. Figure 3.11 shows the linear relationship between the predicted and measured CRs. The function has a zero intercept, a slope of 0.9979 and r^2 of 0.9998. Thus, the shield count obtained under the same conditions as the measurements is useful normalizing the N.

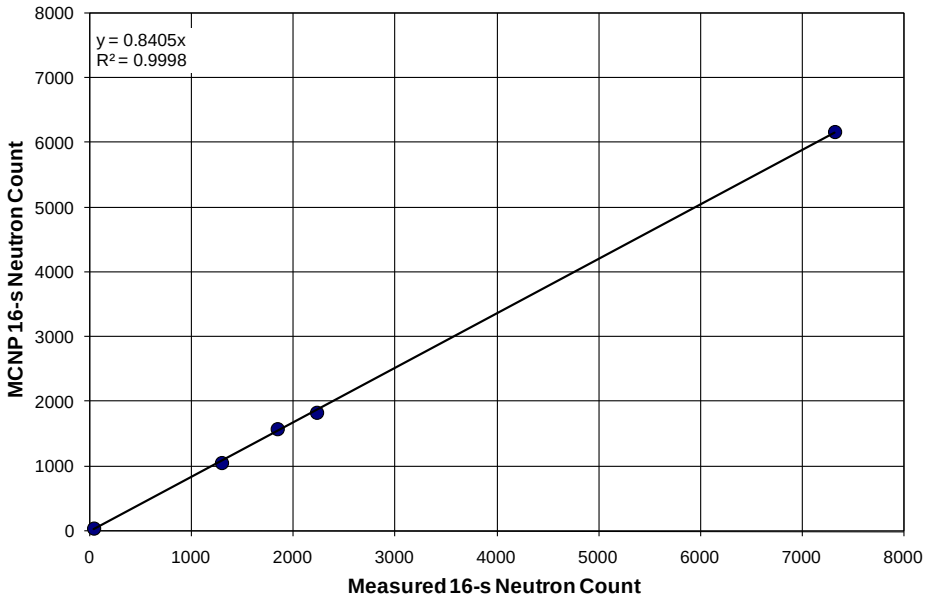

Figure 3.9. Relationship Between MCNP-predicted and Measured N in 8-in. Well

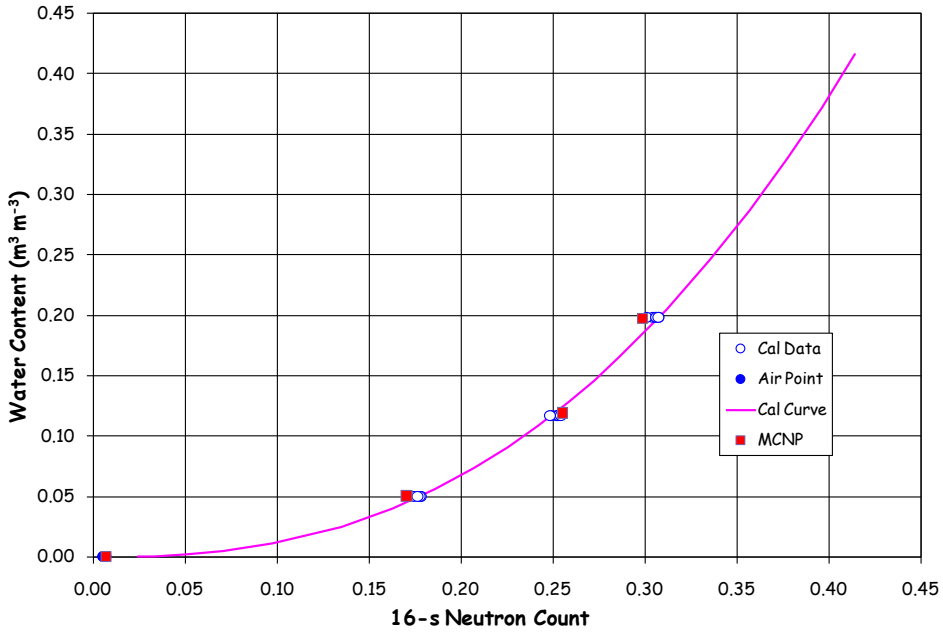

Figure 3.10. Water Content vs. MCNP-Predicted CR in an 8-in. Well

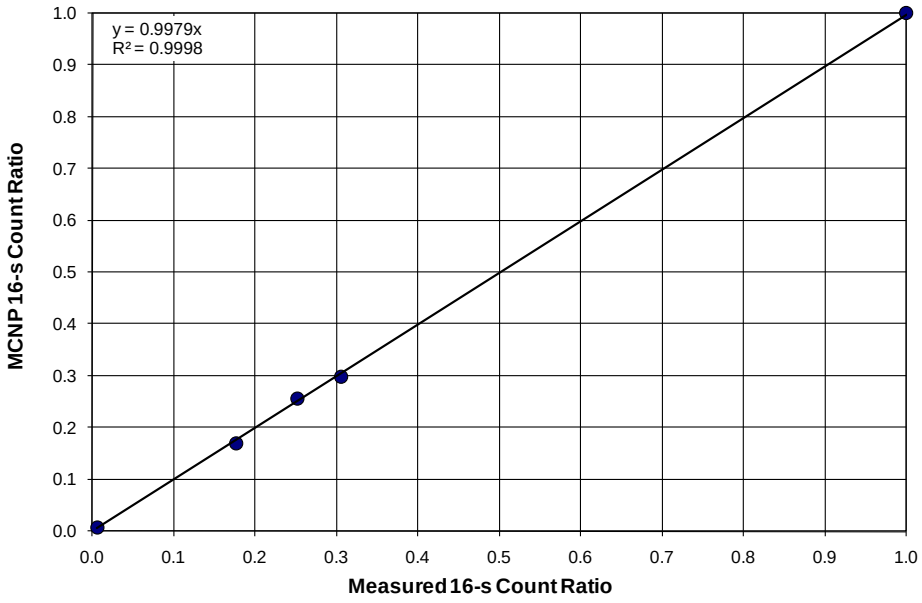

Figure 3.11. Relationship Between MCNP-predicted and Measured CR in 8-in. Well

3.3 MCNP Simulation with 2.5-inch Access Tubes

With a successful match between the MCNP simulations of neutron counts in the three calibration models, the next step was to simulate the response in the smaller 2.5-in. steel cased wells. The steel wells have an internal diameter of 2.125 in. and an outside diameter of 2.5 in. Simulations were performed for all of the calibration models assuming 2-in. wells. In addition, virtual models with $\theta = 0.25$ m^3m^{-3}, $\theta = 0.30$ m^3m^{-3}, $\theta = 0.35$ m^3m^{-3}, and $\theta = 0.40$ m^3m^{-3} were included in the simulations. These virtual models are designated as models H, I, J, and K, respectively, all with dry bulk densities of 1700 kg/m^3.

Table 3.8 shows results of the MCNP simulations in the 2.5-in. wells. Since the air measurement does not assume an access tube in the model, the simulated response for air remains unchanged. Simulations in water, however, assumed a water-filled calibration tank and therefore included an access tube. In water, the predicted N increased from 2458 with 8-in. wells and 4032 with the 6-in. wells to 10836 with the 2-in. wells. Such an increase can be expected as the measurement geometry, particularly the air gap between the probe and the access tube, can have a significant impact on N. A similar effect of the well diameter can be expected in measurements and simulations in the calibration models. Owing to the high value of N in pure water, calculation of CR based on N_s will give rise to CRs > 1.0. A better approach to dealing with differences in N_s and CR > 1 may be use a large common standard like a water drum. In this way the count rates of different probes of the same type can be normalized on the same basis, the same soil calibration can be used for probes of the same design.

Table 3.8. Simulated Neutron Counts for the Calibration Models all with 2.5-in. Steel Wells

Model	θ (m^3 m^{-3})	Bulk Density (kg m^{-3})	MCNP 16-s N	MCNP 16-s CR
Shield		900	6168.72	1.0000
Air	0.000	1.205	14.43	0.0023
A	0.050	1760	2899.05	0.4700
B	0.197	1700	6426.53	1.0418
C	0.119	1760	4957.55	0.8037
E	0.118	1740	4912.18	0.7963
F	0.050	1760	2899.05	0.4700
G	0.198	1700	6426.53	1.0418
H	0.250	1700	7125.29	1.1551
I	0.300	1700	7846.93	1.2721
J	0.350	1700	8419.18	1.3648
K	0.400	1700	8919.46	1.4459
Water	1.000	997.1	10836.31	1.7567

Figure 3.12 shows a plot of MCNP-predicted θ(CR) and the fitted calibration curve. The fitted model parameters and standard errors are summarized in Table 3.9 (Model 1). Figure 3.13 compares the MCNP-simulated 16-s neutron count in the 2-in. access tube with that simulated in the 6-in. tube using the calibration models. The most striking observation is that the neutron counts in the 2-in. access tube are significantly higher than those in the 6-in. wells. This is due to a variety of geometry related factors including wall thickness of the steel well, the smaller air gap between the probe and the well. As shown these data are well-described by a polynomial function.

Table 3.9. Fitted Model Parameters for Calibration Measurements in 2-in. Access Tubes

Model	Equation	A	ε(A)	B	ε (B)
1	$\theta(N) = e^{A} \cdot N^{B}$	-17.9364	0.4554	1.8648	0.0522
2	$^{\dagger}\theta(CR) = e^{A} \cdot CR^{B}$	-1.6622	0.0173	1.8648	0.0522
3	$^{\ddagger}\theta(CR) = e^{A} \cdot CR^{B}$	-0.6115	0.0344	1.8648	0.0522

θ = volumetric water content ($m^3 m^{-3}$); N = 16-s neutron count ; CR = 16-s neutron CR,
†= counts in shield use as standard to calculate CR
‡= counts in water use as standard to calculate CR

Nonetheless, as with the 6-in. wells, there is a monotonic increase in 16-s CR as water content increases. In general, the fit of Equation 2.9 to the data is quite good although the model slightly over-predicts CR at a θ=0.40 m^3 m^{-3}. Figure 3.14 shows a plot of MCNP-predicted θ(CR) and the fitted calibration curve. The fitted model parameters and standard errors are summarized in Table 3.9 (Model 2). This equation provides a good fit to the MCNP-predicted CR values based on using the shield count, N_s, as the standard. As mentioned, another approach is to use measurement in a water drum as the standard. Figure 3.15 shows a plot of MCNP-predicted θ(CR) in which the predicted N in water is used at the standard. The fitted model parameters and standard errors are summarized in Table 3.9 (Model 3). Either of these equations could be used to translating field-measured N to volumetric water content for the T-106 Interim Barrier.

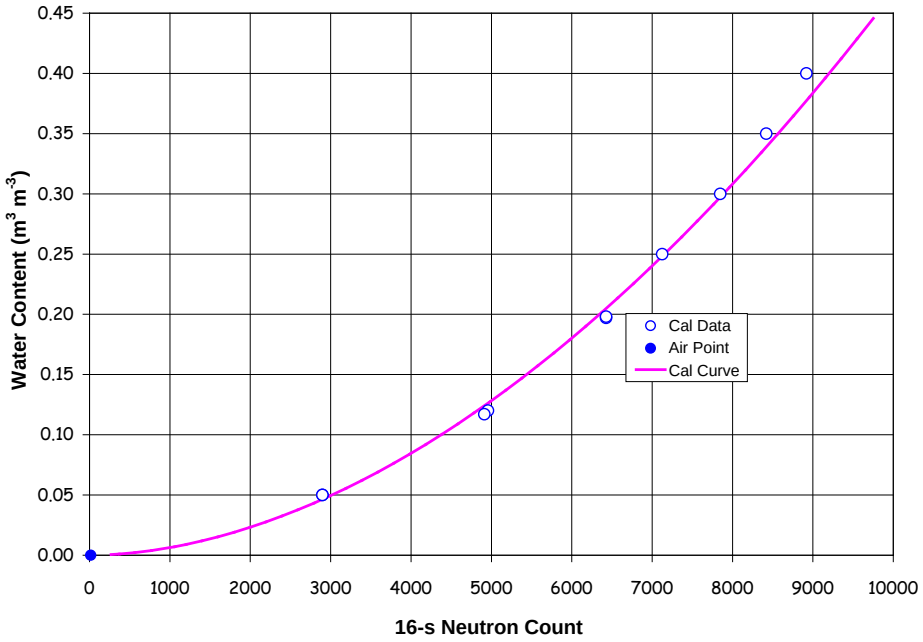

Figure 3.12. Water Content vs. MCNP-Predicted N in a 2.5-in. Well

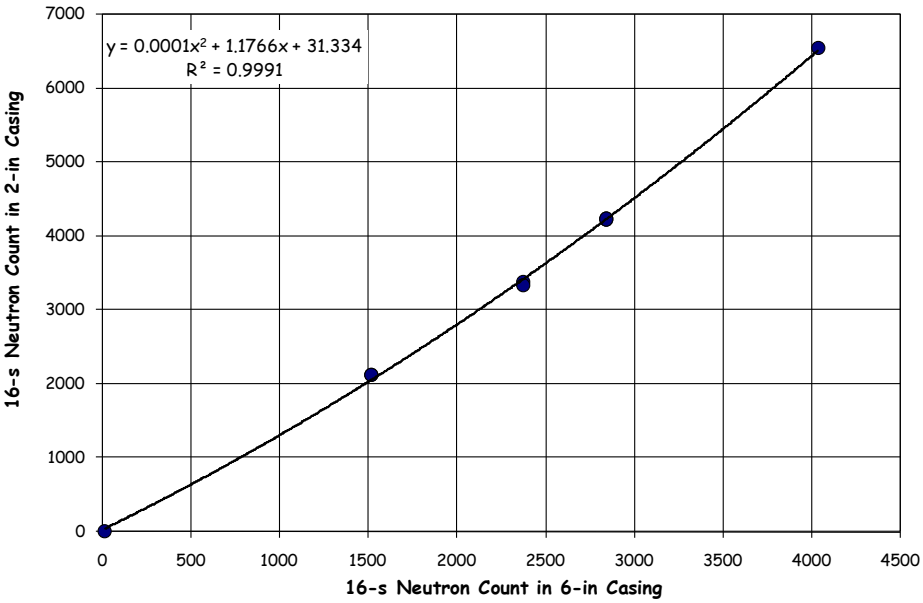

Figure 3.13. Relationship Between MCNP-Simulated 16-s Neutron Count in 2-in. and 6-in. Access Tubes

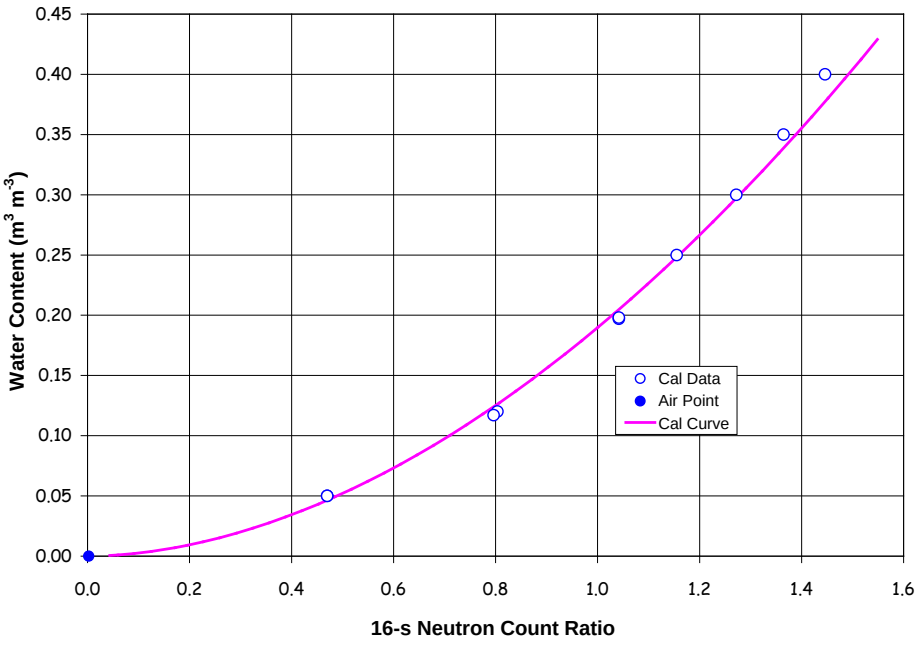

Figure 3.14. Water Content vs. MCNP-Predicted CR in a 2.5-in. Well. CR from Shield Standard

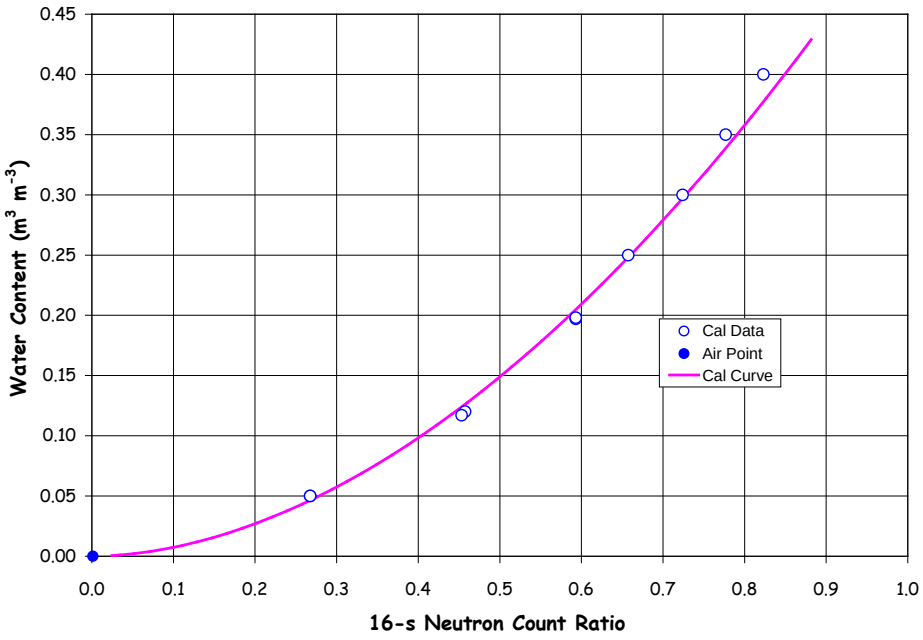

Figure 3.15. Water Content vs. MCNP-Predicted CR in a 2.5-in. Well. CR from Water Standard

3.4 Application to Field Data

To illustrate use of the calibration function and possible error in use of the wrong function, neutron probe data collected from the interim barrier on July 30, 2008 are used. The reported shield count N_s 6341, very similar to the 6168 reported for the calibration measurements in the physical models with the 6-in. wells. Raw counts were converted to count ratios, CR, for each well and then converted to volumetric water content using the calibration curve based on measurements in the 6-in. wells and the new MCNP-based curves for the 2-in. wells. The calculated CRs ranged from 0.357 to 1.031 in well C5307; from 0.08 to 0.62 in C5312; from 0.12 to 0.72 in C5696; and from 0.13 to 0.63 in C5699. A CR > 1.0 in C5307 suggest $N > N_s$ which cannot be explained at this time.

Figure 3.17 shows the water content profiles calculated using the calibration curve based on measurements in the calibration models with 6-in. wells. Water content ranged from 0.111 to 1.03 $m^3\ m^{-3}$ (103.0 vol.%) in C5307; 0.004 to 0.357 $m^3\ m^{-3}$ in C5312; from 0.01 to 0.478 $m^3\ m^{-3}$ in C5696; and from 0.013 to 0.363 $m^3\ m^{-3}$ in C5699. Overall, predicted water content ranges from 0.004 to 1.03 $m^3\ m^{-3}$ with a mode of 0.166 $m^3\ m^{-3}$. These values are inconsistent with what has been observed in similar sediments at Hanford. Engleman et al. (1995) examined a database of over 3600 gravimetric moisture contents for Hanford Formation sediments and reported that values typically ranged from 0.04 and 0.40 $m^3\ m^{-3}$, with a mode of 0.05 $m^3\ m^{-3}$.

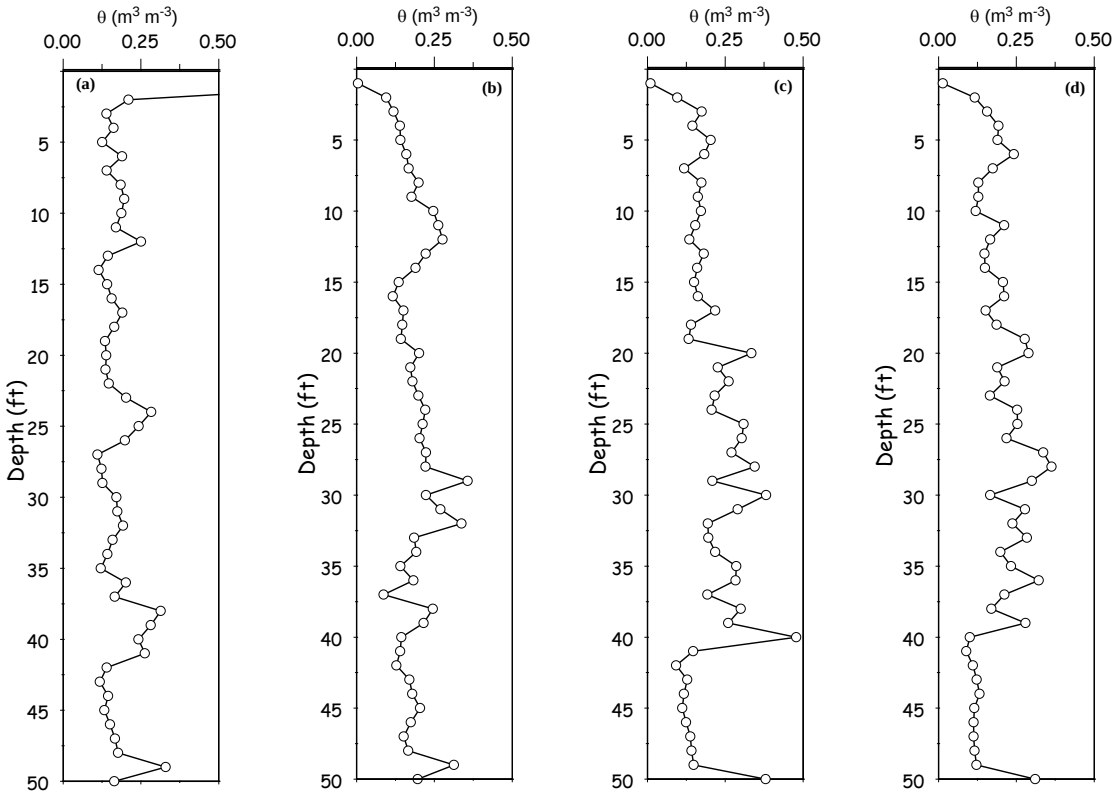

Figure 3.16. Water Content Profiles for Interim Cover on July 30, 2008 with 6-in Well Function, (a) C5307, (b) C5312, (c) C5696, and (d) C5699.

Figure 3.17 shows the water content profiles calculated using the calibration curve based on measurements in the calibration models with 2-in. wells. Water content ranged from 0.03 to 0.20 m^3 m^{-3} in C5307; 0.002 to 0.08 m^3 m^{-3} in C5312; from 0.003 to 0.102 m^3 m^{-3} in C5696; and from 0.004 to 0.08 m^3 m^{-3} in C5699. Overall, predicted water content ranges from 0.002 to 0.201 m^3 m^{-3} with a mode of 0.04 m^3 m^{-3}. These values are certainly more consistent with the observations of Engleman et al. (1995) and those reported for similar sediments at Hanford

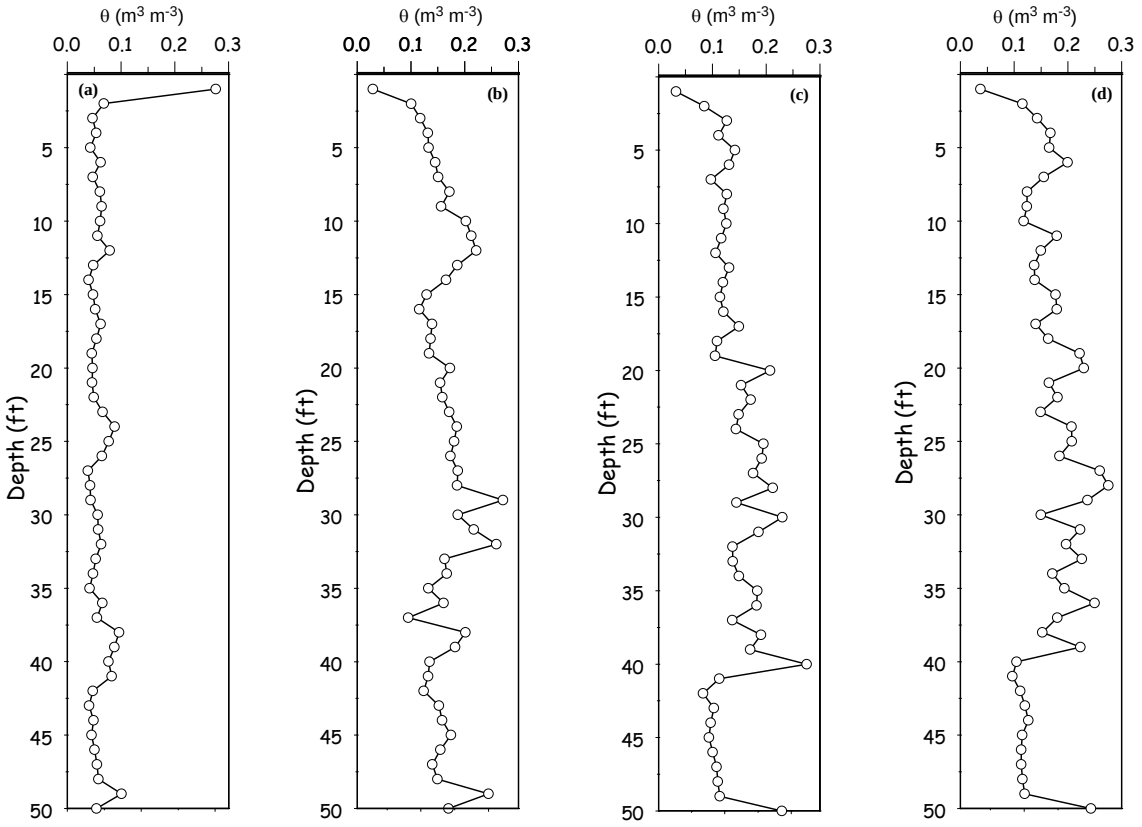

Figure 3.17. Water Content Profiles for Interim Cover on July 30, 2008 with 2-in. Well Function , (a) C5307, (b) C5312, (c) C5696, and (d) C5699.

4.0 Summary and Conclusions

An innovative approach to minimizing recharge in tank farms was recently demonstrated in the form of an interim barrier at Hanford's T Tank Farm. The barrier is composed of multiple layers, including a layer of clean Hanford soil overlain by a geotextile layer and a 0.25-in.-thick layer of polyurea at the surface. Volumetric soil moisture content in the vadose zone beneath the barrier is one of the primary variables being monitored to assess effectiveness. One of the methods being used to determine water content is the neutron hydroprobe. The neutron probe measures the number of thermalized neutrons as a function of depth in the 2-in. access tubes. Computing the soil moisture content from neutron probe counts requires a calibration relationship, but none exists for 2-in. tubes. The objective of this work was to develop a calibration relation for converting neutron counts measured in 2-in. access tubes to soil water content.

A number of calibration options are available for the neutron probe, including vendor calibration, field calibration, and theoretical calibrations based on neutron diffusion theory. The calibration method chosen for this study was a computational approach based on Monte Carlo techniques. The MCNP, developed by Los Alamos, was chosen to perform the theoretical analyses of neutron diffusion in air, the probe shield, and in the Hanford calibration models.

The mean 16-s neutron count measured in air was 43, the mean count for Model F (θ = 0.05 m^3m^{-3}) was 1515, and Model E (θ = 0.117 m^3m^{-3}) and Model G (θ = 0.198 m^3m^{-3}) generated mean 16-s counts of 2264 and 2887, respectively. The shield count, typically used as a standard count to compute the CR, was 6168. The best-fit model relating water content to neutron counts was an exponential model that was essentially equivalent to that currently being used for 6-in. steel-cased wells. The MCNP simulations successfully predicted the neutron CR for the neutron shield and the three calibration models for which data were collected in the field. However, predictions for air (mean 16-s count= 14) were about 65% lower than the measured counts (mean 16-s count =43). This discrepancy can be attributed to uncertainties in the configuration and model geometry used for the air measurements. MCNP-simulated counts for the physical models were essentially equal to the measured counts with values of 2370, 1515, and 2840 for models E, F, and G, respectively.

Successfully predicting the response in 6-in. and 8-in. wells in the three calibration models was motivation to predict the response in 2-in. access tubes. Simulations were performed for six of the seven calibration models as well as four virtual models with the entire set covering a moisture range of 0 to 0.40 m^3m^{-3}. Predicted counts for the calibration models with 2-in. access tubes were 40 to 50% higher than in the 6-in. tubes. Predicted counts for water were about 60% higher in the 2-in. tube than in the 6-in. tube. The discrepancy between the 2-in. and 6-in. wells can be attributed to differences in the geometry, particularly the smaller air gap with the 2-in. wells and differences in wall thickness. The calibration function for the 2-in. access tube is of the same form as that for the 6-in. tube but has different coefficients. The best-fit model relating volumetric water content (θ) to CR is of the form $\theta = e^A \cdot CR^B$ with A=-1.6622 ± 0.0173 and B=1.8648 ± 0.0522. It is recommended that the calibration function based on the CR, rather than raw counts, be used to avoid the effects variable shield counts owing variations environmental conditions and measurement geometry. Owing to the occurrence of CR values > 1.0, a better approach to dealing with differences in N_s and CR > 1 may be use a large common standard like a water drum. In this way the count rates of different probes of the same type can be normalized on the

same basis, the same soil calibration can be used for probes of the same design. Water contents predicted with the new MCNP-based calibration for the 2-in. wells 2-in. ranged from 0.002 to 0.201 m^3 m^{-3} with a mode of 0.04 m^3 m^{-3}. This is more consistent with the observed range of 0.04 and 0.40 m^3 m^{-3} and a mode of 0.05 m^3 m^{-3} observed in Hanford Formation Sediments. These results suggest that the MCNP code can be used to extend calibrations for the neutron probe to different conditions, including access tube size as well as composition, without the need to construct additional physical models.

These results suggest that the MCNP code can be used to extend calibrations for the neutron probe to different conditions, including access tube size as well as composition without the need to construct additional physical models.

5.0 References

Alger RP, S Locke, WA Nagel and H Sherman. 1971. "The Dual Spacing Neutron Log- CNL." Paper SPE-3565, presented at the 1971 SPE Annual Meeting, New Orleans, Louisiana.

Bell JP and JSC McCulloch. 1969. "Soil moisture estimation by the neutron method in Britain." *J. Hydrol.* 7:415–433.

Briesmeister JF. 2000. *MCNP: A General Monte Carlo N-particle Transport Code, Version 4C.* LA-13709-M, Los Alamos National Laboratory, Los Alamos, New Mexico.

Campbell Pacific Nuclear, Inc. (CPN). 1992. *Manufacturers Instructions for CPN 503 Hydroprobe*, CPN, Martinez, California.

Carneiro C and E deJong. 1985. ''In situ determination of the slope of the calibration curve of a neutron probe using a volumetric technique." *Soil Sci.* 139(3):250–254.

Chanasyk DS and MA Naeth. 1996. "Field measurement of Soil Moisture using Neutron Probes." *Can. J. Soil Sci.* 76:317–323.

Cotecchia V, A Inzaghi, E Pirastru, and R Ricchena. 1968. "Influence of the Physical and Chemical Properties of Soil on Measurements of Water Content Using Neutron Probes." *Water Resour. Res.* 4(5):1023–1028

Couchat P, C Carré, J Marcesse, and J Le Ho. 1975. "The measurement of thermal neutron constants of the soil: application to the calibration of neutron moisture gauges and to the pedagogical study of the soil." In: RA. Schraeke and CD. Bowman (Ed), *Nuclear cross sections and technology*. Proceedings of the Conference on Nuclear Data Cross Sections on Technology, March 3-7,Washington, D.C.

Dickey GL. 1990. "Factors affecting neutron meter calibration." In *Irrigation and Drainage*. Proceedings of the 1990 National Conference. Durango, CO, 11-13 July 1990. Harris, S.R. Ed. American Society of Civil Engineers, New York, NY. Pp. 9-20

Dickey GL and LJ Schwankl. 1980. "Soil moisture monitoring using the neutron probe." U.S. Department of Agriculture (USDA)-Soil Conservation Service, Davis, California.

Engelman RE, RE Lewis, DC Stromswold, and JR Hearst. 1995. *Calibration Models for Measuring Moisture in Unsaturated Formations by Neutron Logging*. PNL-10801, Pacific Northwest National Laboratory, Richland, Washington.

Gilchrist Jr, WA, JE Galford, C Flaum, and PD Soran. 1986. "Improved Environmental Corrections for Compensated Neutron Logs." Paper SPE-15540, presented at the 1986 Society of Petroleum Engineers Annual Technical Conference and Exhibition, New Orleans, Louisiana.

Goncalves IF, J Salgado, J Neves and FG Carvalho. 1994. Calibration and design optimization of a nuclear surface moisture-density gauge by Monte Carlo Simulation." *Nuclear Geophysics* 8(6):527–537.

Greacen EL, RL Correll, RB Cunningham, GG Johns, and KD Nicholls. 1981. "Calibration." Pages 50–57 in E. L. Greacen, ed. *Soil water assessment by the neutron method*. Commonwealth Scientific and Industrial Research Organisation, Australia .

Hodnett MG, and JP Bell. 1991. “Neutron Probe Standards: Transport Shields or A Large Drum of Water?” *Soil Sci.* 151(2):113-185

International Atomic Energy Agency (IAEA). 1970. “Neutron Moisture Gauges.” Tech. Rep. Ser. No. 112, Vienna, Austria.

International Organization for Standardization (ISO). 2001. “Reference Neutron Radiations- part 1: Characteristics and Methods of Production.” ISO 8529-1:2001(E), Geneva, Switzerland.

Kristensen KJ. 1973. “Depth intervals and topsoil moisture measurement with the neutron depth probe.” *Nordic Hydrol.* 4:77–85.

Lewis TJ. 1958. “The electric strength and molecular structure of liquids.” *British Journal of Applied Physics* 9:30–33.

Li J, DW Smith, SG Fityus, and D Sheng. 2003. “Numerical Analysis of Neutron Moisture Probe Measurements.” *International Journal of Geomechanics* 3(1):11–20.

McMahon WJ. 2007. “Performance simulation of an interim surface barrier over the 242-T-106 Tank Release.” In: AE Bauer, *Design Analysis for T-Farm Interim Surface Barrier (TISB)*, Appendix A, RPP-33431 Rev. 0, CH2M HILL Hanford Group, Inc., Richland, Washington.

Meisner JE. 1995. Vadose Zone Moisture Measurement Through Steel Casing Evaluation.” WHC-SD-EN-TI-304, Rev. 0, Westinghouse Hanford Company, Richland, Washington.

Meisner JE, RK Price, and RR Randall. 1996. *Radionuclide Logging System In Situ Vadose Zone Moisture Measurement Calibration*. WHC-SD-EN-TI-306, Rev. 0, Westinghouse Hanford Company, Richland, Washington.

Olgaard PL. 1965. *On the theory of the neutronic method for measuring the water content of soil*. Danish Atomic Energy Commission, Riso Rep. 97.

Rawls W J and LE Asmussen. 1973. “Neutron probe field calibration for soils in the Georgia Coastal Plain.” *Soil Sci.* 116:262–265.

Rivard MJ, BM Coursey, LA DeWerd, WF Hanson, SM Huq, GS Ibbott, MG Mitch, R Nath, and JF Williamson. 2004. Update of AAPM Task Group No. 43. Report: “A revised AAPM protocol for brachytherapy dose calculations.” *Medical Physics* 31(3):633–74.

Schmugge TJ, TJ Jackson, and HL McKim. 1980. “Survey of methods for soil moisture determination.” *Water Resour. Res.* 16:961–979.

Schwankl LJ. 1995. Calibration and Use of the Neutron Soil Moisture Gauge, University of California Cooperative Extension

Silvestri V, G Sarkis, N Bekkouche, M Soulie, and C Tabib. 1991. “Laboratory and field calibration of a neutron depth moisture gauge for use in high water content soils.” *Geotech. Test. J.* 14(1):64–70.

Stone JF. 1990. "Neutron physics considerations in moisture probe design." Proceedings of the National Conference of Irrigation and Drainage Division, American Society of Civil Engineers, New York, 1–8.

Stone, JF, HR Gray, DL Weeks. 1995. "Calibration of neutron moisture probes by transfer through laboratory media. II: Stability experience." *Soil Sci*. 160(3): 164-175

Vachaud G, JM Royer, and JD Cooper. 1977. "Comparison of methods of calibration of a neutron probe by gravimetry of neutron-capture model." *Journal of Hydrology*, Amsterdam, 34:343–56.

Ward AL, GW Gee, and SO Link. 1997. *Hanford Prototype Barrier Status Report: FY 1997*. PNNL-11789, Pacific Northwest National Laboratory. Richland, Washington.

Ward AL, JK Linville, JM Keller, and GH Seedahmed. 2005. *200-BP-1 Prototype Hanford Barrier Annual Monitoring Report for Fiscal Year 2004*. PNNL-14960. Pacific Northwest National Laboratory. Richland, Washington.

Ward AL, TC Caldwell, and GW Gee. 2000. *Vadose Zone Transport Field Study: Soil Water Content Distribution by Neutron Moderation*. PNNL-13795, Pacific Northwest National Laboratory, Richland, Washington.

Ward AL, SO Link, CE Strickland, KE Draper, and RE Clayton. 2008. *200-BP-1 Prototype Hanford Barrier Annual Monitoring Report for Fiscal Years 2005 Through 2007*. PNNL-17176, Pacific Northwest National Laboratory, Richland, Washington.

Williams III, RG, CJ Gesh, and RT Pagh. 2006. *Compendium of Material Composition Data for Radiation Transport Modeling*. PNNL-15870, Pacific Northwest National Laboratory, Richland, Washington.

Wilson BF, and PA Wichmann. 1974. "The compensated neutron log and the effects of environment." *Society of Petroleum Engineers of the American Institute of Mining, Metallurgical, and Petroleum Engineers*, Paper SPE 5118, 18 p.

Zhang ZF, JM Keller, and CE Strickland. 2007. *T Tank Farm Interim Surface Barrier Demonstration – Vadose Zone Monitoring Plan*. PNNL-16538, Pacific Northwest National Laboratory, Richland, Washington.

Appendix A

Example MCNP Input for Air Simulations

Appendix A: Example MCNP Input for Air Simulations

```
Air Calibration 0% MC (air), No Shield, Probe suspended in Air
c zd =   +90.0000 cm
c E=3.0Mev
c cells, material, density,relative location
 1    1  -5      -1    8 -9        $Source
 2    7  -15.6   -2    8 -10 #1    $Tungsten carbide
 3    9  -0.0008 -3   13 -16       $He-3 Detector at 6 atm
 4    6  -0.9    14  -15  4  -5    $Polyethylene Moderator
 5    4  -8.0    13  -16  3  -4    $Stainless Steel Side Det
 6    4  -8.0    16  -17 -4        $Stainless Steel Top Det
 7    4  -8.0    12  -13 -4        $Stainless Steel Bottom Det
 8    2  -0.0013  8  -18 -5 #1 #2 #3 #4 #5 #6 #7  $Air
 9    5  -2.699   8  -18  5  -6    $Al Side
10    5  -2.699  18  -19 -6        $Al Top
11    5  -2.699   7  -8  -6        $Al Bottom
12    2  -0.0013 22  -25 -20 #(-19 7 -6 ) $Air
13   10  -7.87   22  -25  20 -21   $Carbon steel Access Tube
14    2  -0.0013 21  -26  23 -24   $Soil Layer 2
15    2  -0.0013 21  -26  24 -25   $Soil Layer 1
16    2  -0.0013 21  -26  22 -23   $Soil Layer 3
17    4  -8      20  -26  25 -27   $Stainless Steel Top
18    4  -8     -26   28 -22       $Stainless Steel Bottom
19    0  -28    :27 :26 :(-20 25 ) $Outside
c
c---Surface Cards
c   surf.no,type,dimension
 1 cz  0.4763     $cylinder on z-axis, r=0.4763
 2 cz  0.8255     $cylinder on z-axis, r=0.8255
 3 cz  1.016      $cylinder on z-axis, r=1.016
 4 cz  1.27       $cylinder on z-axis, r=1.016
 5 cz  1.6942     $cylinder on z-axis, r=1.6942
 6 cz  1.905      $cylinder on z-axis, r=1.905
 7 pz -106.5570   $plane normal to z-axis, z=-106.5570
 8 pz -106.3030   $plane normal to z-axis, z=-106.3030
 9 pz -105.0330   $plane normal to z-axis, z=-105.0330
10 pz -104.3726   $plane normal to z-axis, z=-104.3726
11 pz -103.7630   $plane normal to z-axis, z=-103.7630
12 pz -102.1120   $plane normal to z-axis, z=-102.1120
13 pz -101.6040   $plane normal to z-axis, z=-101.6040
14 pz -100.2705   $plane normal to z-axis, z=-100.2705
15 pz  -97.0955   $plane normal to z-axis, z= -97.0955
16 pz  -88.3960   $plane normal to z-axis, z= -88.3960
17 pz  -87.8880   $plane normal to z-axis, z= -87.8880
18 pz  -80.2680   $plane normal to z-axis, z= -80.2680
19 pz  -80.0140   $plane normal to z-axis, z= -80.0140
20 cz   4.445     $cylinder on z-axis (Access Tube),r=4.445
21 cz   6.370     $cylinder on z-axis (Access Tube),r=6.370
22 pz -190.00     $plane normal to z-axis, z=-190.00
23 pz -122.60     $plane normal to z-axis, z=-122.60
24 pz -77.3       $plane normal to z-axis, z=-77.30
```

```
25 pz 0.0         $plane normal to z-axis, z= 0.0
26 cz 75.0        $plane normal to z-axis, z= 75.0
27 pz 0.635       $plane normal to z-axis, z= 0.635
28 pz -190.635    $plane normal to z-axis, z=-190.635

mode n
imp:n 1. 1. 1. 1. .01 .01 .01 .01 .01 .01 .01 1. 1. 1. 1. 1. .01 .01  0.
c
sdef erg=d1 wgt=3.7e7 pos=0. 0. 0.
    rad=d2 ext=d3 axs=0. 0. 1. par=1 cel=1
c
c---  AmBe volume source defined by ISO 8529-1
c     (Normalized to 1 mCi Am-241 or 2220 neutrons/s)
c
  si1 h 4.140E-07  1.100E-01  3.300E-01  5.400E-01  7.500E-01  9.700E-01
       1.180E+00  1.400E+00  1.610E+00  1.820E+00  2.040E+00  2.250E+00
       2.470E+00  2.680E+00  2.900E+00  3.110E+00  3.320E+00  3.540E+00
       3.750E+00  3.970E+00  4.180E+00  4.390E+00  4.610E+00  4.820E+00
       5.040E+00  5.250E+00  5.470E+00  5.680E+00  5.890E+00  6.110E+00
       6.320E+00  6.540E+00  6.750E+00  6.960E+00  7.180E+00  7.390E+00
       7.610E+00  7.820E+00  8.030E+00  8.250E+00  8.460E+00  8.680E+00
       8.890E+00  9.110E+00  9.320E+00  9.530E+00  9.750E+00  9.960E+00
       1.018E+01  1.039E+01  1.060E+01  1.082E+01  1.100E+01
  sp1 d 0.00      1.44E-02  3.34E-02  3.13E-02  2.81E-02  2.50E-02
       2.14E-02  1.98E-02  1.75E-02  1.92E-02  2.23E-02  2.15E-02
       2.25E-02  2.28E-02  2.95E-02  3.56E-02  3.69E-02  3.46E-02
       3.07E-02  3.00E-02  2.69E-02  2.86E-02  3.18E-02  3.07E-02
       3.33E-02  3.04E-02  2.74E-02  2.33E-02  2.06E-02  1.82E-02
       1.77E-02  2.04E-02  1.83E-02  1.63E-02  1.67e-02  1.68E-02
       1.88E-02  1.84E-02  1.69E-02  1.44E-02  9.68E-03  6.52E-03
       4.26E-03  3.67E-03  3.81E-03  5.06E-03  6.25E-03  5.52E-03
       4.68E-03  3.70E-03  2.78E-03  1.51E-03  3.63E-04
si2 0. .4764
si3  -106.3040  -105.0320
c
m1    95241.50c        0.0714  $Am-Be (1:13) Source
      4009.50c         0.9286
c Air, Dry (RH =0) At sea level
m2    1001          -0.000000 $ H
      6000          -0.000124 $ C
      7014          -0.755268 $ N
      8016          -0.231781 $ O
      18000         -0.012827 $ Ar
m4    6000.60c        -0.0003  $SS-304,SS-304L (with ENDF-VI)
      14000.35c       -0.005 15031.60c     -0.000225 16000.60c      -0.00015
      24050.60c      -0.00793 24052.60c     -0.159031 24053.60c     -0.018378
      24054.60c     -0.004661 25055.60c         -0.01 26054.60c     -0.039996
      26056.60c     -0.644764 26057.60c     -0.015026 26058.60c     -0.002039
      28058.60c      -0.06234 28060.60c     -0.024654 28061.60c     -0.001085
      28062.60c     -0.003504 28064.60c     -0.000917
m5    13027.35c           -1  $aluminum
m6    1001.35c      -0.143711  $polyethylene
      6000.60c      -0.856289
m7    74182.60c     -0.130293  $Tungsten Carbide
      74183.60c     -0.071135 74184.60c     -0.153765 74186.60c     -0.144808
      6000.60c          -0.5
```

```
m9    2003.35c              1  $He-3
m10   6000.60c        -0.0006  $carbon steel with ENDF-VI
      25055.60c       -0.0035 26054.60c     -0.056755 26056.60c      -0.91493
      26057.60c     -0.021323 26058.60c     -0.002893
c
fc34 volume average integrated flux*E**(-0.5) tally for cell 3
f34:n 3
de34   1.e-10 1.e-8 1.e-6 1.e-4 1.e-2 1.e-0 1.e+2 1.e+4 1.e+6 1.e+8
df34   1.e+5  1.e+4 1.e+3 1.e+2 1.e+1 1.e-0 1.e-1 1.e-2 1.e-3 1.e-4
fm34   2.806e-4  $ Flux/E^(1/2) Multipier to get proton counts per 16s
fc11 surface tally
*f11:n 3
e11 1.e-9  2.e-7  3.0
fc14 average flux tally for cell 3
f14:n 3
e14 1.e-9 1.e-8 2.e-8 3.e-8 4.e-8 5.e-8 6.e-8 7.e-8 8.e-8 9.e-8  &
       1.e-7 1.2e-7 1.4e-7 1.6e-7 2.e-7 3.e-7 4.e-7 5.e-7     &
       6.e-7 7.e-7 8.e-7 9.e-7 1.e-6 5.e-6 1.e-5 1.e-4 1.e-3  &
       1.e-2 1.e-1 1.e0 3.0
ctme 1200
```

Appendix B

Example MCNP Input for Shield Simulations

Appendix B: Example MCNP Input for Shield Simulations

```
Model Shield Count
c  Probe surrounded by Si-based paraffin
c
c E=3.0 MeV
 1     1      -5 -1 8 -9  $Source
 2     7   -15.6 -2 8 -10 #1  $Tungsten carbide
 3     9 -0.0008 -3 13 -16  $He-3 Detector at 6 atm
 4     6   -0.930 14 -15 4 -5  $Poly Mod
 5     4    -7.92 13 -16 3 -4  $Stainless Steel Side Det
 6     4    -7.92 16 -17 -4  $Stainless Steel Top Det
 7     4    -7.92 12 -13 -4  $Stainless Steel Bottom Det
 8     2 -0.001205 8 -18 -5 #1 #2 #3 #4 #5 #6 #7  $Air
 9     5 -2.6989   8 -18 5 -6  $Al Side
10     5 -2.6989  18 -19 -6  $Al Top
11     5 -2.6989   7 -8 -6  $Al Bottom
12     2 -0.001205  #(-19 7 -6) #(6 30 -31 32 -33 35 -38) &
                  28 30 -31 32 -33 -25 $Air
13     4 -8.0 6  30 -31 32 -33 35 -36
14     4 -8.0 6  30 -31 32 -33 (-40:41:-42:43) 36 -38
15     4 -8.0 6  -34 36 -37
16    10 -1.05 #14 #15 #13 6 30 -31 32 -33 35 -38
17     0 -28:-30:31:-32:33:25 $Void Outside

1 cz  .4763
2 cz  .8255
3 cz  1.016
4 cz  1.27
5 cz  1.6942
6 cz  1.905
7 pz   -28.5570
8 pz   -28.3030
9 pz   -27.0330
10 pz   -26.3726
12 pz   -24.1120
13 pz   -23.6040
14 pz   -22.2705
15 pz   -19.0955
16 pz   -10.3960
17 pz    -9.8880
18 pz    -2.2680
19 pz    -2.0140
20 cz 10.15
21 cz 10.97
22 pz -190.
23 pz -122.6
24 pz -77.3
25 pz 0.
26 cz 75.
27 pz 0.635
28 pz -50.0
```

```
30 px -8.636
31 px  8.636
32 py -8.636
33 py  8.636
34 cz  3.175
35 pz -34.272
36 pz -31.732
37 pz -26.652
38 pz -19.413
40 px -8.336
41 px  8.336
42 py -8.336
43 py  8.336

mode n
c Importance Card
imp:n 1. 15r  0.
c
c Source Specification Card
c
sdef erg=d1 wgt=141367 pos=0. 0. 0.
    rad=d2 ext=d3 axs=0. 0. 1. par=1 cel=1
c
c  Souce Information Card for Distribution 1 (ERG)
c  AmBe volume source defined by ISO 8529-1, Table A.4
c  Normalized to 1 mCi Am-241 or 2220 neutrons/s
c
 si1 h 4.140E-07  1.100E-01  3.300E-01  5.400E-01  7.500E-01  9.700E-01
      1.180E+00  1.400E+00  1.610E+00  1.820E+00  2.040E+00  2.250E+00
      2.470E+00  2.680E+00  2.900E+00  3.110E+00  3.320E+00  3.540E+00
      3.750E+00  3.970E+00  4.180E+00  4.390E+00  4.610E+00  4.820E+00
      5.040E+00  5.250E+00  5.470E+00  5.680E+00  5.890E+00  6.110E+00
      6.320E+00  6.540E+00  6.750E+00  6.960E+00  7.180E+00  7.390E+00
      7.610E+00  7.820E+00  8.030E+00  8.250E+00  8.460E+00  8.680E+00
      8.890E+00  9.110E+00  9.320E+00  9.530E+00  9.750E+00  9.960E+00
      1.018E+01  1.039E+01  1.060E+01  1.082E+01  1.100E+01
c
c  Souce Probability Card for Distribuition 1 (ERG)
c
sp1 d   0.00     1.44E-02  3.34E-02  3.13E-02  2.81E-02  2.50E-02
      2.14E-02  1.98E-02  1.75E-02  1.92E-02  2.23E-02  2.15E-02
      2.25E-02  2.28E-02  2.95E-02  3.56E-02  3.69E-02  3.46E-02
      3.07E-02  3.00E-02  2.69E-02  2.86E-02  3.18E-02  3.07E-02
      3.33E-02  3.04E-02  2.74E-02  2.33E-02  2.06E-02  1.82E-02
      1.77E-02  2.04E-02  1.83E-02  1.63E-02  1.67e-02  1.68E-02
      1.88E-02  1.84E-02  1.69E-02  1.44E-02  9.68E-03  6.52E-03
      4.26E-03  3.67E-03  3.81E-03  5.06E-03  6.25E-03  5.52E-03
      4.68E-03  3.70E-03  2.78E-03  1.51E-03  3.63E-04
c
c  Source information for distribution 2 (Distance from POS)
c
si2 0.0 0.4764
c
c  Source information for distribution 3 (Distance from POS along AXS)
c
si3   -28.3040   -27.0320
```

```
c
c Material Cards
c
m1    95241.60c        0.0714  $Am-Be (1:13) Source
      4009.60c         0.9286
c Air, Dry (near sea level), rho=0.001205 g/cc
m2    6000           -0.000124 $ C
      7014           -0.755268 $ N
      8016           -0.231781 $ O
      18000          -0.012827 $ Ar
c Steel, Stainless 204, rho=7.92 g/cc
m4    24000          -0.190 $Cr
      25055          -0.020 $Mn
      26000          -0.695 $Fe
      28000          -0.095 $Ni
m5    13027          -1.000000  $aluminum
c Normal polyethylene, rho=0.930 g/cc
m6    1001           -0.143716  $H
      6012           -0.856284  $C
c Tungsten Carbide
m7    74182.60c      -0.130293
      74183.60c      -0.071135
      74184.60c      -0.153765
      74186.60c      -0.144808
       6000          -0.5
m9    2003.60c       1  $He-3
c Si-based Paraffin wax, (CH3)3-Si-[O-Si(CH3)2]n-O-Si-(CH3)3 for large n, rho=1.05 g/cc
m10   6012           0.20 $C
      8016           0.10 $O
      1001           0.65 $H
      14000          0.05 $Si
c
c Tally Specification Card
c
fc34 integrated flux*E**(-0.5) tally for cell 3 (counts per sec/cm^3)
f34:n 3
de34   1.e-10 1.e-8 1.e-6 1.e-4 1.e-2 1.e-0 1.e+2 1.e+4 1.e+6 1.e+8
df34   1.e+5  1.e+4 1.e+3 1.e+2 1.e+1 1.e-0 1.e-1 1.e-2 1.e-3 1.e-4
fm34   1.365e-4  $ Flux/E^(1/2) Multipier to get proton counts per sec/cm^3
fc24 average (n,p) reaction rate tally in cell 3 (counts per sec/cm^3)
f24:n 3
fm24 -1 9 103   $ He3(n,p)T reaction rate for mat9 (He3)
e24 1.e-9 1.e-8 2.e-8 3.e-8 4.e-8 5.e-8 6.e-8 7.e-8 8.e-8 9.e-8  &
       1.e-7 1.2e-7 1.4e-7 1.6e-7 2.e-7 3.e-7 4.e-7 5.e-7     &
       6.e-7 7.e-7 8.e-7 9.e-7 1.e-6 5.e-6 1.e-5 1.e-4 1.e-3  &
       1.e-2 1.e-1 1.e0 3.0 10.0 20.0
fc11 surface tally
*f11:n 3
e11 1.e-9  2.e-7  3.0 10.0 20.0
fc14 average flux tally for cell 3
f14:n 3
e14 1.e-9 1.e-8 2.e-8 3.e-8 4.e-8 5.e-8 6.e-8 7.e-8 8.e-8 9.e-8  &
       1.e-7 1.2e-7 1.4e-7 1.6e-7 2.e-7 3.e-7 4.e-7 5.e-7     &
       6.e-7 7.e-7 8.e-7 9.e-7 1.e-6 5.e-6 1.e-5 1.e-4 1.e-3  &
       1.e-2 1.e-1 1.e0 3.0 10.0 20.0
c
```

```
c Time or History Card
c
c ctme 1200   $Computing time cutoff in minutes
nps 10000000  $Maximum number of histories
```

Appendix C

Example MCNP Input for Water Simulations

Appendix C: Example MCNP Input for Water Simulations

```
Model A 100% Water; Access Tube=2.5 in. carbon steel
c    zd =   -95.0000
c E=3.0Mev
 1     1      -5 -1 8 -9  $Source
 2     7   -15.6 -2 8 -10 #1  $Tungsten carbide
 3     9 -0.0008 -3 13 -16  $He-3 Detector at 6 atm
 4     6   -0.930 14 -15 4 -5  $Poly Mod
 5     4    -7.92 13 -16 3 -4  $Stainless Steel Side Det
 6     4    -7.92 16 -17 -4  $Stainless Steel Top Det
 7     4    -7.92 12 -13 -4  $Stainless Steel Bottom Det
 8     2 -0.001205 8 -18 -5 #1 #2 #3 #4 #5 #6 #7  $Air
 9     5 -2.6989   8 -18 5 -6  $Al Side
10     5 -2.6989  18 -19 -6  $Al Top
11     5 -2.6989   7 -8 -6  $Al Bottom
12     2 -0.001205 22 -25 -20 #(-19 7 -6 ) $Air
13    10 -7.82 22 -25 20 -21  $Carbon steel Access Tube
14     3  -0.9971 21 -26 23 -24  $ Layer 2 water
15     3  -0.9971 21 -26 24 -25  $ Layer 1 water
16     3  -0.9971 21 -26 22 -23  $ Layer 3 water
17     4  -7.92 20 -26 25 -27  $Stainless Steel Top
18     4  -7.92 -26 28 -22  $Stainless Steel Bottom
19     0         -28 :27 :26 :(-20 25 ) $Outside

1 cz  .4763
2 cz  .8255
3 cz  1.016
4 cz  1.27
5 cz  1.6942
6 cz  1.905
7 pz  -106.5570
8 pz  -106.3030
9 pz  -105.0330
10 pz  -104.3726
11 pz  -103.7630
12 pz  -102.1120
13 pz  -101.6040
14 pz  -100.2705
15 pz   -97.0955
16 pz   -88.3960
17 pz   -87.8880
18 pz   -80.2680
19 pz   -80.0140
20 cz 5.3975 $Access Tube ID
21 cz 6.35 $Access Tube OD
22 pz -190.
23 pz -122.6
24 pz -77.3
25 pz 0.
26 cz 75.
27 pz 0.635
```

```
28 pz -190.635

mode n
c Importance Card
imp:n 1. 17r  0.
c
c Source Specification Card
c
sdef erg=d1 wgt=141367 pos=0. 0. 0.
    rad=d2 ext=d3 axs=0. 0. 1. par=1 cel=1
c
c  Souce Information Card for Distribution 1 (ERG)
c  AmBe volume source defined by ISO 8529-1, Table A.4
c  Normalized to 1 mCi Am-241 or 2220 neutrons/s
c
  si1 h 4.140E-07  1.100E-01  3.300E-01  5.400E-01  7.500E-01  9.700E-01
       1.180E+00  1.400E+00  1.610E+00  1.820E+00  2.040E+00  2.250E+00
       2.470E+00  2.680E+00  2.900E+00  3.110E+00  3.320E+00  3.540E+00
       3.750E+00  3.970E+00  4.180E+00  4.390E+00  4.610E+00  4.820E+00
       5.040E+00  5.250E+00  5.470E+00  5.680E+00  5.890E+00  6.110E+00
       6.320E+00  6.540E+00  6.750E+00  6.960E+00  7.180E+00  7.390E+00
       7.610E+00  7.820E+00  8.030E+00  8.250E+00  8.460E+00  8.680E+00
       8.890E+00  9.110E+00  9.320E+00  9.530E+00  9.750E+00  9.960E+00
       1.018E+01  1.039E+01  1.060E+01  1.082E+01  1.100E+01
c
c  Souce Probability Card for Distribuition 1 (ERG)
c
sp1 d   0.00      1.44E-02  3.34E-02  3.13E-02  2.81E-02  2.50E-02
       2.14E-02  1.98E-02  1.75E-02  1.92E-02  2.23E-02  2.15E-02
       2.25E-02  2.28E-02  2.95E-02  3.56E-02  3.69E-02  3.46E-02
       3.07E-02  3.00E-02  2.69E-02  2.86E-02  3.18E-02  3.07E-02
       3.33E-02  3.04E-02  2.74E-02  2.33E-02  2.06E-02  1.82E-02
       1.77E-02  2.04E-02  1.83E-02  1.63E-02  1.67e-02  1.68E-02
       1.88E-02  1.84E-02  1.69E-02  1.44E-02  9.68E-03  6.52E-03
       4.26E-03  3.67E-03  3.81E-03  5.06E-03  6.25E-03  5.52E-03
       4.68E-03  3.70E-03  2.78E-03  1.51E-03  3.63E-04
c
c  Source information for distribution 2 (Distance from POS)
c
si2 0.0 0.4764
c
c  Source information for distribution 3 (Distance from POS along AXS)
c
si3  -106.3040  -105.0320
c
c Material Cards
c
m1    95241.60c        0.0714  $Am-Be (1:13) Source
      4009.60c         0.9286
c Air, Dry (near sea level), rho=0.001205 g/cc
m2    6000           -0.000124 $ C
      7014           -0.755268 $ N
      8016           -0.231781 $ O
      18000          -0.012827 $ Ar
c Water, 100%,rho=0.9971 g/cc
m3    1001           -0.111894
```

```
     8016         -0.888106
c Steel, Stainless 204, rho=7.92 g/cc
m4    24000         -0.190 $Cr
      25055         -0.020 $Mn
      26000         -0.695 $Fe
      28000         -0.095 $Ni
m5    13027         -1.000000  $aluminum
c Normal polyethylene, rho=0.930 g/cc
m6    1001          -0.143716  $H
      6012          -0.856284  $C
c Tungsten Carbide
m7    74182.60c     -0.130293
      74183.60c     -0.071135
      74184.60c     -0.153765
      74186.60c     -0.144808
       6000         -0.5
c
m9    2003.60c       1  $He-3
c Carbon steel
m10   6012          -0.005  $C
      26000         -0.995  $Fe
c
c Tally Specification Card
c
fc34 integrated flux*E**(-0.5) tally for cell 3 (counts per sec/cm^3)
f34:n 3
de34   1.e-10 1.e-8 1.e-6 1.e-4 1.e-2 1.e-0 1.e+2 1.e+4 1.e+6 1.e+8
df34   1.e+5  1.e+4 1.e+3 1.e+2 1.e+1 1.e-0 1.e-1 1.e-2 1.e-3 1.e-4
fm34   1.365e-4  $ Flux/E^(1/2) Multipier to get proton counts per sec/cm^3
fc24 average (n,p) reaction rate tally in cell 3 (counts per sec/cm^3)
f24:n 3
fm24 -1 9 103   $ He3(n,p)T reaction rate for mat9 (He3)
e24 1.e-9 1.e-8 2.e-8 3.e-8 4.e-8 5.e-8 6.e-8 7.e-8 8.e-8 9.e-8  &
       1.e-7 1.2e-7 1.4e-7 1.6e-7 2.e-7 3.e-7 4.e-7 5.e-7     &
       6.e-7 7.e-7 8.e-7 9.e-7 1.e-6 5.e-6 1.e-5 1.e-4 1.e-3  &
       1.e-2 1.e-1 1.e0 3.0 10.0 20.0
fc11 surface tally
*f11:n 3
e11 1.e-9  2.e-7  3.0 10.0 20.0
fc14 average flux tally for cell 3
f14:n 3
e14 1.e-9 1.e-8 2.e-8 3.e-8 4.e-8 5.e-8 6.e-8 7.e-8 8.e-8 9.e-8  &
       1.e-7 1.2e-7 1.4e-7 1.6e-7 2.e-7 3.e-7 4.e-7 5.e-7     &
       6.e-7 7.e-7 8.e-7 9.e-7 1.e-6 5.e-6 1.e-5 1.e-4 1.e-3  &
       1.e-2 1.e-1 1.e0 3.0 10.0 20.0
c
c Time or History Card
c
c ctme 1200   $Computing time cutoff in minutes
nps 10000000  $Maximum number of histories
```

Appendix D

Example MCNP Input for Calibration Model Simulations

Appendix D: Example MCNP Input for Calibration Model Simulations

```
Model E 12% MC, Density=1.74 g/cm^3 Access Tube=2.5 in. carbon steel
c    zd =   -95.0000
c E=3.0Mev
 1     1      -5 -1 8 -9  $Source
 2     7   -15.6 -2 8 -10 #1  $Tungsten carbide
 3     9 -0.0008 -3 13 -16  $He-3 Detector at 6 atm
 4     6    -0.9 14 -15 4 -5  $Poly Mod
 5     4    -8.0 13 -16 3 -4  $Stainless Steel Side Det
 6     4    -8.0 16 -17 -4  $Stainless Steel Top Det
 7     4    -8.0 12 -13 -4  $Stainless Steel Bottom Det
 8     2 -0.001205  8 -18 -5 #1 #2 #3 #4 #5 #6 #7  $Air
 9     5 -2.699   8 -18 5 -6  $Al Side
10     5 -2.699  18 -19 -6  $Al Top
11     5 -2.699   7 -8 -6  $Al Bottom
12     2 -0.001205 22 -25 -20 #(-19 7 -6 ) $Air
13    10 -7.87 22 -25 20 -21  $Carbon steel Access Tube
14     3  -1.740 21 -26 23 -24  $ Layer 2
15     8  -1.740 21 -26 24 -25  $ Layer 1
16     8  -1.740 21 -26 22 -23  $ Layer 3
17     4      -8 20 -26 25 -27  $Stainless Steel Top
18     4      -8 -26 28 -22  $Stainless Steel Bottom
19     0         -28 :27 :26 :(-20 25 ) $Outside

1 cz  .4763
2 cz  .8255
3 cz  1.016
4 cz  1.27
5 cz  1.6942
6 cz  1.905
7 pz  -106.5570
8 pz  -106.3030
9 pz  -105.0330
10 pz  -104.3726
11 pz  -103.7630
12 pz  -102.1120
13 pz  -101.6040
14 pz  -100.2705
15 pz   -97.0955
16 pz   -88.3960
17 pz   -87.8880
18 pz   -80.2680
19 pz   -80.0140
20 cz  5.3975 $Access Tube ID
21 cz  6.35 $Access Tube OD
22 pz -190.
23 pz -122.6
24 pz -77.3
25 pz 0.
26 cz 75.
```

```
27 pz 0.635
28 pz -190.635

mode n
c Importance Card
imp:n 1. 17r  0.
c
c Source Specification Card
c
sdef erg=d1 wgt=141367 pos=0. 0. 0.
    rad=d2 ext=d3 axs=0. 0. 1. par=1 cel=1
c
c  Souce Information Card for Distribution 1 (ERG)
c  AmBe volume source defined by ISO 8529-1, Table A.4
c  Normalized to 1 mCi Am-241 or 2220 neutrons/s
c
  si1 h 4.140E-07  1.100E-01  3.300E-01  5.400E-01  7.500E-01  9.700E-01
       1.180E+00  1.400E+00  1.610E+00  1.820E+00  2.040E+00  2.250E+00
       2.470E+00  2.680E+00  2.900E+00  3.110E+00  3.320E+00  3.540E+00
       3.750E+00  3.970E+00  4.180E+00  4.390E+00  4.610E+00  4.820E+00
       5.040E+00  5.250E+00  5.470E+00  5.680E+00  5.890E+00  6.110E+00
       6.320E+00  6.540E+00  6.750E+00  6.960E+00  7.180E+00  7.390E+00
       7.610E+00  7.820E+00  8.030E+00  8.250E+00  8.460E+00  8.680E+00
       8.890E+00  9.110E+00  9.320E+00  9.530E+00  9.750E+00  9.960E+00
       1.018E+01  1.039E+01  1.060E+01  1.082E+01  1.100E+01
c
c  Souce Probability Card for Distribuition 1 (ERG)
c
sp1 d   0.00      1.44E-02  3.34E-02  3.13E-02  2.81E-02  2.50E-02
       2.14E-02  1.98E-02  1.75E-02  1.92E-02  2.23E-02  2.15E-02
       2.25E-02  2.28E-02  2.95E-02  3.56E-02  3.69E-02  3.46E-02
       3.07E-02  3.00E-02  2.69E-02  2.86E-02  3.18E-02  3.07E-02
       3.33E-02  3.04E-02  2.74E-02  2.33E-02  2.06E-02  1.82E-02
       1.77E-02  2.04E-02  1.83E-02  1.63E-02  1.67e-02  1.68E-02
       1.88E-02  1.84E-02  1.69E-02  1.44E-02  9.68E-03  6.52E-03
       4.26E-03  3.67E-03  3.81E-03  5.06E-03  6.25E-03  5.52E-03
       4.68E-03  3.70E-03  2.78E-03  1.51E-03  3.63E-04
c
c  Source information for distribution 2 (Distance from POS)
c
si2 0.0 0.4764
c
c  Source information for distribution 3 (Distance from POS along AXS)
c
si3  -106.3040  -105.0320
c
c Material Cards
c
m1    95241.60c        0.0714  $Am-Be (1:13) Source
      4009.60c         0.9286
c Air, Dry (near sea level), rho=0.001205 g/cc
m2    6000           -0.000124 $ C
      7014           -0.755268 $ N
      8016           -0.231781 $ O
      18000          -0.012827 $ Ar
c $Al(OH)3 + Silicaceous sand, 11.7% WC,rho=1.74 g/cc
```

```
m3    13027        -0.0674
      8016         -0.5259    1001        -0.0075   14000.60c     -0.2696
      26000        -0.0156   20000.60c     -0.0670   12000.60c     -0.0103
      11023.60c     -0.0056   19000.60c     -0.0109   6012         -0.0201
      25055        -0.0006
c Steel, Stainless 204, rho=7.92 g/cc
m4    6000         -0.0003
      14000.60c       -0.005 15031.60c     -0.000225 16000.60c      -0.00015
      24050.60c      -0.00793 24052.60c     -0.159031 24053.60c      -0.018378
      24054.60c     -0.004661 25055         -0.01 26054.60c     -0.039996
      26056.60c     -0.644764 26057.60c     -0.015026 26058.60c      -0.002039
      28058.60c      -0.06234 28060.60c     -0.024654 28061.60c     -0.001085
      28062.60c     -0.003504 28064.60c     -0.000917
c  aluminum, rho=2.6989 g/cc
m5    13027     -1.00000
c  polyethylene, rho=0.930
m6    1001      -0.143711
      6000      -0.856289
c Tungsten Carbide, rho=15.6 g/cc
m7    74182.60c     -0.130293
      74183.60c     -0.071135 74184.60c     -0.153765 74186.60c     -0.144808
      6000         -0.5
c $Al(OH)3 + Silicaceous sand, 11.7% WC,rho=1.74 g/cc
m8    13027     -0.0674
      8016         -0.5259   1001      -0.0075   14000.60c     -0.2696
      26000        -0.0156   20000.60c     -0.0670   12000.60c     -0.0103
      11023.60c     -0.0056   19000.60c     -0.0109   6012         -0.0201
      25055        -0.0006
c Helium-3, rho=0.0008 g/cc
m9    2003.60c       1.0000
c Carbon steel
m10   6012          -0.005  $C
      26000        -0.995  $Fe
c
c Tally Specification Card
c
fc34 integrated flux*E**(-0.5) tally for cell 3 (counts per sec/cm^3)
f34:n 3
de34   1.e-10 1.e-8 1.e-6 1.e-4 1.e-2 1.e-0 1.e+2 1.e+4 1.e+6 1.e+8
df34   1.e+5  1.e+4 1.e+3 1.e+2 1.e+1 1.e-0 1.e-1 1.e-2 1.e-3 1.e-4
fm34   1.365e-4  $ Flux/E^(1/2) Multipier to get proton counts per sec/cm^3
fc24 average (n,p) reaction rate tally in cell 3 (counts per sec/cm^3)
f24:n 3
fm24 -1 9 103   $ He3(n,p)T reaction rate for mat9 (He3)
e24 1.e-9 1.e-8 2.e-8 3.e-8 4.e-8 5.e-8 6.e-8 7.e-8 8.e-8 9.e-8  &
       1.e-7 1.2e-7 1.4e-7 1.6e-7 2.e-7 3.e-7 4.e-7 5.e-7     &
       6.e-7 7.e-7 8.e-7 9.e-7 1.e-6 5.e-6 1.e-5 1.e-4 1.e-3  &
       1.e-2 1.e-1 1.e0 3.0 10.0 20.0
fc11 surface tally
*f11:n 3
e11 1.e-9  2.e-7  3.0 10.0 20.0
fc14 average flux tally for cell 3
f14:n 3
e14 1.e-9 1.e-8 2.e-8 3.e-8 4.e-8 5.e-8 6.e-8 7.e-8 8.e-8 9.e-8  &
       1.e-7 1.2e-7 1.4e-7 1.6e-7 2.e-7 3.e-7 4.e-7 5.e-7     &
       6.e-7 7.e-7 8.e-7 9.e-7 1.e-6 5.e-6 1.e-5 1.e-4 1.e-3  &
```

```
      1.e-2 1.e-1 1.e0 3.0 10.0 20.0
c
c Time or History Card
c
c ctme 1200   $Computing time cutoff in minutes
nps 10000000  $Maximum number of histories
```

Distribution

(Issued on Electronically)

No. of Copies

1 Flor Federal Services
R. Khaleel R3-50

2 CH2M-Hill Plateau Remediation Company, Inc.
GD Cummins H8-15
CD Wittreich H8-15

2 Washington River Protection Solutions
MP Bergeron S7-66
JG Field R2-51
DJ Meyer S5-03

1 SM Stoller Corporation
R McCain S7-66

1 Three Rivers Scientific
RR Randall
2345 Stevens Drive, Rm. 1100
Richland, WA 99354

No. of Copies

1 Energy Solutions
K Reynolds
2521 Stevens Drive, Rm. 520
Richland, WA 99354

9 Local Distribution
Pacific Northwest National Laboratory
RE Clayton K6-75
WJ Greenwood K9-33
N Hasan K9-33
ME Rockhold K9-33
CE Strickland K9-33
ES Sullivan K6-81
RS Wittman K9-33
ZF Zhang K9-33
AL Ward K9-33
Information Release Office (PDF)

Pacific Northwest
NATIONAL LABORATORY

U.S. DEPARTMENT OF
ENERGY

902 Battelle Boulevard
P.O. Box 999
Richland, WA 99352
1-888-375-PNNL (7665)
www.pnl.gov